Age-specific mechanisms regulate neural crest and mesodermal contribution to the enteric nervous system in health and disease

Subhash Kulkarni[1#], Monalee Saha[1], Laren Becker[2], Alpana Singh[1], Jared Slosberg[3], Chengxiu Zhang[1], Alicia Bukowski[1], Zhuolun Wang[1], Guosheng Liu[1], Jenna Leser[1,] Mithra Kumar[1], Shriya Bakhshi[1], Matthew Anderson[4], Mark Lewandoski[4], Sushma Nagaraj[1], Elizabeth Vincent[3], Loyal A. Goff [3, 5, 6], Pankaj Jay Pasricha[1]

[1]Center for Neurogastroenterology, Department of Medicine, Johns Hopkins University – School of Medicine, Baltimore, MD 21205

[2]Division of Gastroenterology, Stanford University – School of Medicine, Stanford CA 94301

[3]Department of Genetic Medicine, Johns Hopkins University – School of Medicine, Baltimore, MD 21205

[4]Center for Cancer Research, National Cancer Institute, Frederick, MD 21702

[5]Department of Neuroscience, Johns Hopkins University – School of Medicine, Baltimore, MD 21205

[6]Kavli Neurodiscovery Institute, Johns Hopkins University – School of Medicine, Baltimore, MD 21205

[#]Address all correspondence to:

Subhash Kulkarni, Ph.D.

Assistant Professor

Department of Medicine

skulkar9@jh.edu

Abstract

The enteric nervous system (ENS), a collection of neurons contained in the wall of the gut, is of fundamental importance to gastrointestinal and systemic health. According to the prevailing paradigm, the ENS arises from progenitor cells migrating from the embryonic neural crest and remains largely unchanged thereafter. Here, we show that the lineage composition of maturing ENS changes with time, with a decline in the canonical lineage of neural-crest derived neurons and their replacement by a newly identified lineage of mesoderm-derived neurons. Single cell transcriptomics and immunochemical approaches establish a distinct expression profile of mesoderm-derived neurons. The dynamic balance between the proportions of neurons from these two different lineages in the post-natal gut is dependent on the availability of their respective trophic signals, GDNF-RET and HGF-MET. With increasing age, the mesoderm-derived neurons become the dominant form of neurons in the ENS, a change associated with significant functional effects on intestinal motility which can be reversed by GDNF supplementation. Transcriptomic analyses of human gut tissues show reduced GDNF-RET signaling in patients with intestinal dysmotility which is associated with reduction in neural crest-derived neuronal markers and concomitant increase in transcriptional patterns specific to mesoderm-derived neurons. Normal intestinal function in the adult gastrointestinal tract therefore appears to require an optimal balance between these two distinct lineages within the ENS.

Introduction

The enteric nervous system (ENS) is a large collection of neurons and related cells that resides within the gastrointestinal wall and regulates gut motility and secretion along with modulating epithelial and immune cell function[1,2]. During fetal development, the mammalian ENS is populated by neurons and glia derived from neural crest (NC)-derived precursors[3-9]. These precursors follow diverse migratory routes to colonize and innervate various parts of the gut before birth[10-12]. It is not clear, however, that this lineage persists in its entirety in the adult gut, as indicated by the observed lack of expression of fluorescent reporter protein in a subpopulation of adult enteric neurons in NC-lineage-traced mice[13,14]. Alternative sources of enteric neurons that have been proposed in the literature include the ventral neural tube (VENT)[15], or the Pdx1-expressing pancreatic endoderm[14], but the interpretation of these studies has been limited by the lack of robust lineage markers for non-NC derived neurons[16]. In addition, while prior studies have documented cellular changes to the ageing ENS[17], the developmental mechanisms behind these changes are unknown. Thus, confirmation of a second, distinct lineage of enteric neurons in adults is important for our understanding of the healthy post-natal development and aging of the ENS, as well as for the pathogenesis of acquired disorders of the ENS.

In this study, we found that while the early post-natal ENS is derived from the canonical NC-lineage, this pattern changes rapidly as the ENS matures, due to the arrival and continual expansion of a novel population of Mesoderm-derived Enteric Neurons (MENs) which represent an equal proportion of the ENS in young adulthood and with increasing age, eventually outnumber the NC-derived Enteric Neurons (NENs). We also found that, while the NEN population is regulated by glial derived neurotrophic factor (GDNF) signaling through its receptor RET, the MEN population is regulated by hepatocyte growth factor (HGF) signaling. Increasing HGF levels during maturation or by pharmacological dosing increase proportions of MENs. Similarly, decrease in

GDNF with age decrease NENs; and increasing GDNF levels by pharmacological dosing increase NENs proportions in the adult ENS to impact intestinal motility.

These results indicate for the first time that the mesoderm is an important source of neurons in the second largest nervous system of the body. The increasing proportion of neurons of mesodermal lineage is a natural consequence of maturation and aging; further, this lineage can be expected to have vulnerabilities to disease that are distinct from those affecting the NEN population. These findings therefore provide a new paradigm for understanding the structure and function of the adult and aging ENS in health, age-related gut dysfunction and other acquired disorders of gastrointestinal motility.

Results

Only half of all mid-age adult enteric neurons are derived from the neural crest. We analyzed small intestinal longitudinal muscle-myenteric plexus (LM-MP) from adult (post-natal day 60; P60) Wnt1-cre:*Rosa26*-tdTomato mice, in which tdTomato is expressed by all derivatives of Wnt1^{+} NC-cells[18]. In these tissues, while GFAP, a glial marker, was always co-expressed with tdTomato (Fig 1A), tdTomato-expression was absent in almost half of all myenteric neurons expressing the pan-neuronal marker HuC/D (tdTomato^{+} neurons: 53.5 ± 3.8 SEM; tdTomato^{-} neurons: 45.92 ± 3.8 SEM; n = 53 ganglia from 5 mice, p = 0.16; Fig 1B, C). In these lineage-traced mice, myenteric ganglia were found to contain tdTomato^{high} and tdTomato^{low} neurons and due care was taken to image subsets (Fig S1A). Both tdTomato^{high} and tdTomato^{low} neurons were classified as tdTomato^{+} and only neurons that did not show any tdTomato-expression were classified as tdTomato^{-} neurons. Additional confirmation was provided by an analogous Wnt1-cre:*Hprt*-tdTomato lineage-traced mouse line, in which tdTomato was expressed from the *Hprt* locus in a Wnt1-cre-dependent manner (*Hprt* locus is X-inactivated in females, hence only adult male mice were used)[19]; and by the Pax3-cre:*Rosa26*-tdTomato lineage-traced mouse line, where

Rosa26-tdTomato driven by the Pax3-cre transgene labels the derivatives of the neural tube and pre-migratory NC (Fig S1B, C)[20]. Similar lack of reporter expression was previously observed in adult myenteric neurons from Sox10-cre NC-lineage-traced mice, confirming our observations of the presence of a significant proportion of non-NC-derived neurons in the adult ENS[13].

Lineage-tracing confirms a mesodermal derivation for half of all adult myenteric neurons. Alternative sources of enteric neurons proposed previously include the ventral neural tube[15], and the pancreatic endoderm[14], but the interpretation of these studies was limited by the lack of robust lineage markers[16]. Brokhman et al[14] found evidence of labeled neurons in inducible Pdx1-cre, Foxa2-cre, and Sox17-cre lineage-traced mouse lines and inferred their derivation from pancreatic endoderm. However, in a Pdx1-cre lineage-traced mouse line, many neuroectoderm-derived neurons of the central nervous system have also been previously shown to be derived from Pdx1-expressing cells[21], suggesting that Pdx1 is not an exclusive endodermal marker. Foxa2 is expressed by mesoderm-derived cells in the heart[22] and Sox17 also labels mesoderm-derived cells, especially cells of the intestinal vasculature[23-26]. We therefore hypothesized that the embryonic mesoderm may be the true developmental source of the non-NC enteric neurons.

Mesoderm-derived cells during embryogenesis express Tek[22] and analysis of LM-MP tissues from adult male Tek-cre:*Hprt*-tdTomato lineage-traced mice revealed the presence of a population of tdTomato^{+} neurons (Fig 2A). Since Tek is not expressed in the adult ENS (Fig S2A), the presence of Tek-derived adult myenteric neurons suggested their mesodermal origin. We then used *mesoderm posterior 1* or Mesp1 as a definitive developmental marker for the embryonic mesoderm[27-31] to confirm the mesodermal derivation of the non-NC derived adult enteric neurons. Reporter expression in this mouse line has been previously studied in cardiac development, which we confirmed by observing its expression in the adult heart tissue (Fig 2B). Expression of tdTomato in both Tek-cre and Mesp1-cre mice was less pronounced in cardiac myocytes (Fig 2B, S2B) and myenteric neurons (Fig 2A, 2C) as compared with vascular cells, which reflects the

variable expression of the reporter gene in both the neural crest- and mesoderm-lineage specific transgenic mouse lines (Fig 2B, 2C, S1A, S2B, S2C). Variable expression of CAG and other pan-cellular promoters in various cell-types and during processes of maturation have previously been reported[32-35]. In addition, an earlier study by Agah et al showed differing degrees of CAG-driven LacZ reporter activation in a cardiac-specific transgenic cre mouse line, which were unrelated to copy number, suggesting insertional and positional effects or, potentially, differential methylation[36]. These reports are consistent with our observation and could potentially help explain the observed variable expression of CAG and CMV promoter-driven reporter genes in our study.

Analysis of small intestinal LM-MP from P60 Mesp1-cre:*Rosa26*-tdTomato lineage-traced mice (Fig 2D, S2C) showed that tdTomato-expression was observed in about half of all myenteric neurons (tdTomato$^+$ neurons: 48.5 ± 5.24 SEM; tdTomato$^-$ neurons: 51.5 ± 5.24 SEM; n = 31 ganglia from 3 mice, p = 0.68) (Fig 2E). Because of the variable expression of the reporter gene in the transgenic mice described above, we also labeled Mesp1-cre:*Rosa26*-tdTomato$^+$ neurons with the S46 antibody, which was raised against the slow tonic myosin heavy chain protein MHCst derived from avian embryonic upper leg muscle, and is expressed exclusively by mesoderm-derived cell populations (Fig 2F)[37-40]. MHCst immunostaining was exclusively observed in all Tek-cre:*Rosa26*-tdTomato$^+$ MENs (Fig S2D) and Wnt1-cre:*Rosa26*-tdTomato$^-$ non-expressing non-NC lineage neurons. Thus. both lineage tracing and protein biomarker expression provides strong support for their mesodermal origin (Fig 2G, Fig S3A). Along with our observations on Wnt1-cre:*Rosa26*-tdTomato mice (Fig 1C), our results indicate that these two distinct lineages together account for all the adult small intestinal myenteric neurons.

The proteins RET, a receptor tyrosine kinase that transduces GDNF signaling in NC-derived enteric neuronal precursors, and MET, a receptor for hepatocyte growth factor (HGF), are expressed by different subsets of adult myenteric neurons[41]. MET is classically expressed by

mesoderm-derived cells[42], and by using immunostaining of small intestinal LM-MP tissues from Wnt1-cre:*Rosa26*-tdTomato and Mesp1-cre:*Rosa26*-tdTomato mice, we found that the expression of MET was restricted to a sub-population of adult MENs (Fig 3A, B). By contrast, RET expression was confined to NENs (Fig 3C).

We then studied whether MENs and NENs differed phenotypically. In the adult murine ENS, inhibitory enteric motor neurons express the nitric oxide-producing enzyme nitric oxide synthase 1 (NOS1); and enteric sensory neurons, called intrinsic primary afferent neurons (IPANs) express the neuropeptide calcitonin gene related peptide (CGRP)[9,41]. Analyses of NOS1 and CGRP expression in the LM-MP from P60 Wnt1-cre:*Rosa26*-tdTomato mice showed that while tdTomato$^+$ neurons account for the majority of NOS1$^+$ inhibitory neurons (NOS1$^+$ tdTomato$^+$: 63.42 ± 3.33 SEM; NOS1$^+$ tdTomato$^-$: 36.58 ± 3.33 SEM; n = 32 ganglia from 3 mice, $p < 0.0001$; Fig 3D, E), tdTomato$^-$ neurons account for the majority of CGRP$^+$ neurons (CGRP$^+$ tdTomato$^-$: 74.36 ± 2.18 SEM; CGRP$^+$ tdTomato$^+$: 25.64 ± 2.18 SEM; n = 30 ganglia from 3 mice, $p < 0.0001$; Fig 3F, G). These results are in keeping with a previous report that show low expression of NOS1 and abundant expression of CGRP by MET$^+$ neurons[41], previously not known to be of a different lineage. The cell size of MENs was significantly larger than that of NENs (n = 143 neurons/group; Feret diameter (µm) MENs: 17.47 ± 0.36 SEM, NENs: 13.05 ± 0.23 SEM, , $p < 0.0001$; Fig S4A), which is consistent with their putative role as IPANs, which are also known consist of large diameter neurons[43]. A sensory role for MENs is also supported by their specific expression of Cadherin-3 (CDH3, Fig 3H, S3B), which marks a sub-population of mechanosensory spinal neurons[44].

An expanded molecular characterization of MENs using unbiased single cell RNA sequencing (scRNAseq)-based analyses. The separate nature of the MENs and NENs was further ascertained by scRNAseq-based analyses on all cells isolated from ileal LM-MP. Unlike

other studies that analyzed either FACS-sorted Wnt1-cre:*Rosa26*-tdTomato^{+} ENS-cells or used classical NENs markers to drive identification of enteric neurons[45,46], we performed agnostic clustering of the scRNAseq data from tissues of two 6-month-old adult male C57BL/6 wildtype mice (Fig S4B, C). We identified the cluster of NC-derived cells by exclusive expression of canonical NC markers Ret and Sox10; and the MENs cluster by its co-expression of the genes Calcb (CGRP), Met, and Cdh3 (Fig 4A; S4B, C). With cells from both samples pooled together, we compared 1,713 NC-derived cells with 2,223 MENs.

Examination of the MENs cluster yielded additional MENs-specific marker genes Slpi, Aebp1, Clic3, Fmo2, Smo, Myl7, and Slc17a9, whose expression by adult enteric neurons has not been previously described (Fig 4B). In addition, the MEN cluster was also enriched in previously characterized ENS markers, such as Ntf3 and Il18[2,47] (Fig 4B). Exclusive expression of Il18 by MENs, which has recently been shown to regulate mucosal immunity[2], indicates a potential immunomodulatory function. We validated the MEN-specificity of these markers using immunochemical analyses (Fig 4C; S3B - K). In addition to these MEN-specific genes, the expression of the pre-synaptic gene Snap25, a component of the SNARE complex, has been reported in all NC-derived Wnt1-cre:tdTomato^{+} enteric neurons (Fig S4E) and in a subset of human ENS neurons[45,48], while it is not detected in the MEN cluster in our analyses (Fig S4F). While the SNAP-25 expressing neurons did express tdTomato in the myenteric ganglia of a Wnt1-cre:*Rosa26*-tdTomato transgenic mouse, they did not express the MENs-marker MHCst, suggesting the NENs-specific expression of this canonical marker for synaptic neurons (Fig 5).

The proportion of mesoderm-derived neurons expands with age to become the dominant population in the aging ENS. Since the ENS at birth consists solely of NENs[13], we next studied the birth-date and eventual expansion of the MEN lineage in the post-natal gut. Using Wnt1-cre:*Rosa26*-tdTomato mouse line, we enumerated the tdTomato^{-} MENs in LM-MP at different

ages and found a significant age-associated increase in MENs proportions ($F = 296.0$, DFn, DFd = 1, 250; $p < 0.0001$) (Fig 6A, B, C). At P11, MENs were found only in few isolated myenteric ganglia (Fig 6A) and together represented only ~5% of all myenteric neurons (n = 34 ganglia from 3 mice), suggesting that they originate shortly before this age. The proportion of MENs in myenteric ganglia rises sharply thereafter: by P22, they account for ~30% of all neurons (n = 45 ganglia from 3 mice); and at P60 they represent ~45% of all neurons (n = 37 ganglia from 3 mice). By P180, MEN comprise 75% of the ENS (n = 60 ganglia from 6 mice) and at very old age, P510, the ENS is populated almost exclusively by MENs (Fig 6B, n = 67 ganglia from 3 mice).

We show that the proportions of NENs and MENs in the myenteric ganglia can be used as a biomarker for deducing ENS age, as a healthy ENS dominant is NENs would be juvenile, one with equal proportions would be adult, and an aging ENS is dominated by MENs.

GDNF and HGF levels regulate the populations of the neural crest-derived and the mesoderm-derived neurons, respectively. GDNF-RET signaling is responsible for proliferation and neurogenesis from NC-derived ENS precursor cells during development as well as for the survival of Ret-expressing enteric neurons[49-52]. Similarly, HGF signaling has been shown to be essential for the proliferation of mesoderm-derived cells[53]. Since the expression of the HGF receptor MET and the GDNF receptor RET is exclusive to MENs and NENs respectively, we studied the correlation between age and levels of HGF and GDNF in LM-MP (Fig 6D, E). We found that while HGF expression increases progressively between P10 and P90 ages (n = 3 mice/age-group, Protein levels: $F = 8.820$, DFn, DFd = 1, 7, $p = 0.02$; mRNA levels: $F = 36.98$, DFn, DFd = 1, 16, $p < 0.0001$) (Fig 6F, G); in agreement with a previous report[53], GDNF expression is markedly reduced between the P10 and the P30 ages and remains reduced thereafter up to the P90 age (n = 3 mice/age-group, $F = 6.821$, DFn, DFd = 1, 7, $p = 0.0348$) (Fig 5H). The ratio of HGF to GDNF expression in ileal LM-MP tissue shows significant increase from

the age of P10 to P90 in our data (Fig S5A), and HGF expression is consistently more than GDNF expression in the full thickness small intestinal tissue from adult and aging mice (Fig S5B).

Since HGF tissue levels increase with age, we hypothesized that increasing HGF signaling drives the expansion of MENs. HGF administration to cohorts of P10 Wnt1-cre:*Rosa26*-tdTomato mice over 10 days promoted an increase in the tdTomato^{-} MENs population in P20 mice to levels previously observed in P60 mice, while tissues from saline-treated control mice exhibited a MENs:NENs ratio that is expected at P20 (n = 99 ganglia from 5 mice for Controls, %MENs: 32.48 ± 2.55 SEM; n = 104 ganglia from 5 mice for HGF treatment, %MENs: 45.38 ± 2.73 SEM; $p < 0.001$) (Fig 6I). Interestingly, HGF-driven ENS maturation did not alter the total numbers of small intestinal myenteric neurons (Fig 6I).

Since GDNF tissue levels are correlated with NENs proportions, we next hypothesized that GDNF signaling regulates NENs proportions in maturing and adult ENS. On administration of GDNF or saline to cohorts of P10 Wnt1-cre:*Rosa26*-tdTomato mice over 10 days[49,54], we found that GDNF treatment promoted the juvenile phenotype by enhancing the proportions of tdTomato^{+} NENs and correspondingly reduced the proportion of tdTomato^{-} MENs in P20 mice to a level similar to that seen at the P10 age (Fig 6J). At the same time, the MENs proportions in saline-treated control mice remained at a level expected of its age (Controls: n = 65 ganglia from 3 mice, %MENs: 79.39 ± 2.97 SEM; GDNF: n = 58 ganglia from 3 mice, %MENs: 94.51 ± 1.75 SEM; $p < 0.0001$) (Fig 6J). Similar to our observations with HGF administration and consistent with a previous report [49], the GDNF-driven expansion of NENs and associated contraction of MENs conserved the total neuronal numbers (Fig 6J). We next tested GDNF's ability to reverse loss of NENs in the adult ENS and found that GDNF administration significantly decreased MENs and increased NENs proportions in P60 male Wnt1-cre:*Rosa26*-tdTomato mice compared to the saline-treated age and strain-matched control mice, while again maintaining total neuronal numbers (Controls: n =

57 ganglia from 3 mice, %MENs: 49.32 ± 2.04 SEM; GDNF: n = 47 ganglia from 3 mice, %MENs: 42.91 ± 1.12 SEM; $p < 0.05$) (Fig 6K).

Reduced GDNF-RET signaling accelerates ENS aging to cause intestinal dysfunction. Since reduced GDNF or RET levels are associated with intestinal dysfunction in patients[55], we hypothesized that alterations in GDNF-RET signaling unrelated to those seen with normal aging, would cause dysfunction. To test this hypothesis, we studied lineage proportions and intestinal function in a mouse model of reduced RET signaling. Ret-null heterozygous mice, which have been previously used to study the effect of reduced RET signaling in the adult ENS, have normal ENS structure but altered gut physiology[49]. A similar mouse model with a Ret^{CFP} allele has a CFP reporter inserted at its *Ret* locus rendering it null[56] and in these mice, we confirmed that the NENs marker Ret-CFP, and the MENs marker MHCst were expressed by different neuronal subpopulations (Fig 7A). Using the adult $Ret^{+/CFP}$ (or $Ret^{+/-}$) mice, we tested the effect of partial Ret loss on ENS lineages at two adult ages: 9 weeks (~P60) and 16 weeks (~P110). $Ret^{+/-}$ mice show a significant reduction in the proportions of Ret-CFP^{+} NENs (9 weeks: n = 37 ganglia from 3 mice, %Ret-CFP^{+} NENs: 25.24 ± 4.2 SEM; 16 weeks: n = 86 ganglia from 5 mice, %Ret-CFP^{+} NENs: 14.02 ± 2.24 SEM; $p < 0.05$) and a corresponding significant increase in the proportions of $MHCst^{+}$ MENs with age, while control $Ret^{+/+}$ mice showed no significant age-associated change in the proportions of MENs (9 weeks $Ret^{+/-}$: n = 38 ganglia from 3 mice, %$MHCst^{+}$ MENs: 62.41 ± 3.83 SEM; 16 weeks $Ret^{+/-}$: n = 55 ganglia from 5 mice, %$MHCst^{+}$ MENs: 84.18 ± 2.53 SEM, $p < 0.0001$); (9 weeks $Ret^{+/+}$: n = 37 ganglia from 3 mice, %$MHCst^{+}$ MENs: 50.85 ± 4.23 SEM; 16 weeks $Ret^{+/+}$: n = 65 ganglia from 5 mice, %$MHCst^{+}$ MENs: 57.77 ± 2.73 SEM, $p = 0.43$) (Fig 7B, C). This expedited loss of NENs in $Ret^{+/-}$ mice confirms that depletion of endogenous RET signaling in the adult ENS accelerates the aging-associated loss of NENs.

Having previously shown that aging mice have intestinal dysmotility[57], we tested whether the increased loss of NENs in the $Ret^{+/-}$ ENS, concomitant with the expansion of MENs accelerated ENS aging, as evidenced by the accelerated expansion of MENs, causes an early onset of aging-associated intestinal dysmotility. We studied intestinal transit in a cohort (n = 8) of adult $Ret^{+/-}$ mice and their littermate control (n = 10) $Ret^{+/+}$ mice over 7 weeks, between 9 and 16 weeks of age. While the 9-week old adult $Ret^{+/-}$ mice had similar whole gut transit times (WGTT) as control $Ret^{+/+}$ mice, WGTT between the two genotypes diverged with age. Consistent with a prior report[49], 16-week old $Ret^{+/-}$ mice displayed significantly delayed intestinal transit compared to age-matched control $Ret^{+/+}$ mice (WGTT (in min) $Ret^{+/+}$: 121.4 ± 4.01 SEM; $Ret^{+/-}$: 157.3 ± 14.62 SEM, $p < 0.05$)(Fig 7D).

GDNF reverts aging in the ENS to normalize intestinal motility. Along with others, we have previously shown that aging is associated with retardation of intestinal motility[58,59]. We hypothesized that this may be a consequence of the replacement of the juvenile NENs population by MENs and therefore GDNF supplementation, by restoring a more balanced MENs:NENs ratio, may prevent age related changes in motility. We studied 17-month-old male mice (at an age where NENs constitute only ~5% of all myenteric neurons; Fig 6C) before and after they received 10 days of intraperitoneal injection of GDNF or saline (n=5 for each cohort). While the two cohorts showed no significant difference in their intestinal transit times at baseline (WGTT (in min) Control: 175.0 ± 11.55 SEM; GDNF: 202.4 ± 7.60 SEM, p = 0.50), GDNF treatment caused significant improvement in intestinal transit (WGTT (in min) Control: 192.8 ± 8.89 SEM; GDNF: 101.0 ± 8.91 SEM, p = 0.0004), reaching levels previously observed in healthy mice (Fig 8A; 7D). GDNF treatment did not change the average neuronal numbers in the ileal myenteric ganglia (n = 50 ganglia/cohort; Control: 18.18 ± 1.54 SEM, GDNF: 16.76 ± 1.25 SEM, p = 0.47), but significantly

reduced the proportions of MHCst^{+} MENs (n = 50 ganglia/cohort; Control: 90.03 ± 1.44 SEM, GDNF: 72.99 ± 3.24 SEM, $p < 0.0001$) while increasing the numbers of RET^{+} NENs (Control: n = 42 ganglia, 1.35 ± 0.14 SEM, GDNF: n = 41 ganglia 3.19 ± 0.31 SEM, $p < 0.0001$) (Fig 8B, C; S6).

MENs in healthy and diseased human gut. To understand the relevance of our observations to human health and disease, we examined the expression of MENs markers MHCst and MET in LM-MP tissues from adult humans with no known gut motility disorder and found them to be expressed by a population of myenteric neurons, suggesting the presence of MENs in normal adult human ENS (Fig 9A; S7). We then queried the plasma proteome levels from the LonGenity cohort of 1,025 aging individuals and found that HGF levels correlated positively, while GDNF and RET levels correlated negatively with age (Fig S8)[60], suggesting parallels between our data (Fig 6) from murine intestine and human plasma proteome data.

Next, we tested whether gut dysfunction associated with pathological reductions in NENs-signaling mechanisms are also associated with increased abundance of MENs. For this, we mined previously generated and publicly available transcriptomic data from control tissues from humans with normal gut motility and from patients with obstructed defecation (OD), which is a chronic intestinal dysmotility disorder[57]. In these datasets, Kim et al have previously shown that OD patients have significantly reduced intestinal expression of Gdnf and Ret[57]. We tested whether the reduced expression of NENs-regulatory genes Gdnf and Ret in OD patients is associated with an increase in MENs-specific transcriptional signature. We have previously published a bioinformatic approach, which allows us to learn latent space representations of gene expression patterns using single cell transcriptomic data, which include patterns that correspond to cell-type-specific gene expression signatures[61]. We can then project new single cell and bulk RNA transcriptomic datasets into these learned patterns to accurately quantify the differential use of these cell-type-specific signatures in transcriptomic data across platforms, tissues, and species[61].

In this instance, gene expression patterns were learned using non-negative matrix factorization (NMF) dimensionality reduction on our murine single cell transcriptomic data. In this manner, our scRNAseq data was decomposed into 50 distinct NMF-patterns[61,62] (Fig 9B). From the reduced set of dimensions, we identified 4-different MENs-specific transcriptional signature patterns by correlation of pattern usage matrix with our cellular annotations (Fig 9B). Next, using our transfer learning tool *ProjectR*[61,63], which allowed us to query bulk-RNAseq data across species to estimate relative use of MENs-specific NMF-patterns, we tested whether the contribution of MENs-specific NMF-patterns was significantly altered between transcriptomes of OD patients and healthy humans (n = 3/group)[57]. This projection indicated that 2 of the 4 MENs-specific NMF-patterns were significantly upregulated in OD samples compared to controls (Student's t-test, $p < 0.05$) (Fig 9C, S9), providing evidence that intestinal dysmotility in OD patients is associated with a relative increase in MENs-specific transcriptional signatures. We further queried the differential gene analyses performed by Kim et al and found that important NEN genes Snap25, Gdnf, Ret, Nos1 were significantly downregulated while the MEN marker genes identified in this study (Clic3, Cdh3, Slc17a9) (Fig S10) were significantly upregulated. The presence of human myenteric neurons expressing MENs markers, along with the altered NENs and MENs-signaling in aging humans, and the relative increase in MENs-specific transcriptomic signatures in patients with gut dysmotility suggests that the lineage dynamics we identify in murine ENS are also of importance in the human ENS.

Discussion

Current dogma states that the adult ENS is exclusively derived from neural crest precursors that populate the gut in early embryonic life[64]. The results of this study indicate a much more complex system, one in which the fetal and early life "juvenile" ENS consisting of neural crest-derived enteric neurons (NENs) is incrementally replaced during maturation by mesoderm-derived enteric neurons (MENs); eventually, the aging ENS consists almost exclusively of the neurons of the

MEN lineage. This study also provides the first definitive evidence of a significant mesodermal contribution to any neural tissue. Previously, the mesoderm and especially the Lateral Plate Mesoderm (LPM) was known to give rise to diverse cell-types within the viscera, including several in the gut[65], and our study shows that cells of this embryonic derivation also give rise to ENS neurons. A previous report on a dual origin of the ENS described adult enteric neurons from Foxa2^{+} or Sox17^{+} precursors[14] and inferred that these were endodermal in origin. However, Foxa2 and Sox17 are also expressed by mesoderm-derived cells[22-25]. By contrast, using two NC-lineage-traced mouse lines (Wnt1-cre and Pax3-cre), two lineage-traced mouse lines marking mesodermal derivatives (Tek-cre, and Mesp1-cre), and robust adult mesoderm markers, we identify a population of Mesp1-derived MHCst- and MET-expressing adult enteric neurons, which makes up the entire non-NC-derived population of myenteric neurons. These results provide evidence that the second source of adult enteric neurons is the mesoderm, and not the endoderm. Importantly, we were also able to confirm MHCst and MET expression in many enteric neurons in adult humans, suggesting that the mesoderm-derived ENS may be a feature common to mice and humans alike. MENs in both species can readily be identified by their expression of MHCst and MET, thus providing a convenient tool to further discriminate and study these neurons.

In our single cell transcriptomic analysis, we used the markers Calcb, Met, and Cdh3 that we had validated to identify and annotate the MEN cell cluster. When compared with the Ret and Sox10-expressing NC-derived cell cluster, an additional set of marker genes were found to be expressed widely or selectively within MENs. Some of these, such as Slpi, Aebp1, Clic3, and Fmo2 have not been previously described in enteric neurons, while others (Ntf3, Il18, and Cftr) are known to be expressed[2,47,66]. The differential expression of genes between the two neuronal populations (MENs versus NENs) suggests putative specialized functional roles of these subpopulations when they co-exist in adults. Some of the prior scRNAseq analysis of post-natal ENS did not detect and characterize the true identity of the MEN lineage. This is because previous studies were

performed either exclusively on neural crest-derived ENS cells[45], or when done in a more agnostic manner, only applied known canonical neural markers to identify the ENS population[46,67]. Another recent study on scRNAseq of enteric neurons detected several neurons with a 'mesenchymal' transcriptomic signature[68]. In this study, May-Zhang et al.[68] show that these 'mesenchymal' neurons exclusively express Ntf3 and Cdh3 which are detected as highly expressed in our MENs scRNAseq dataset. However, May-Zhang-et al did not further interrogate the developmental origins of the 'mesenchymal' enteric neurons to establish the etiology of their distinct transcriptomic signature. Thus, the discovery of the distinct identity and germ-layer derivation of MENs would not have been possible.

Since our scRNAseq data highlighted the lineage-specific nature of the expression of Ret and Met, we studied whether these genes regulated the origin, expansion, and maintenance of the neuronal populations that express them. While it is known that Gdnf expression in the mature gut is significantly downregulated[41,49,54], the functional consequences of this loss have been unclear[49]. We found that reduced GDNF-RET signaling drives the age-dependent loss of NENs as this loss can be slowed or reversed by GDNF supplementation and accelerated by further reduction of Ret expression. In aging animals, GDNF-driven resuscitation of NENs was associated with a functional normalization of age-associated delay in intestinal transit. Our results identify a novel role for GDNF in maintaining or resuscitating the canonical NEN population, while preserving overall enteric neuronal numbers. In the last few years, studies have focused on identifying juvenile protective factors (JPFs), the loss of which correlates with or drives maturation- and aging-associated phenotypes[69]. In this context, GDNF may therefore qualify as a JPF or a *senolytic* as its presence maintains the dominance of NENs in maturing ENS, corresponding to a juvenile phenotype; and its re-introduction promotes and resuscitates the genesis of NENs in adult and aging gut to restore healthy gut function. The exact nature of the cells that respond to

GDNF re-introduction and generate NENs is yet unknown, but it can be hypothesized that these may include Nestin^{+} enteric neural stem cells and/or GDNF-responsive Schwann cells[70,71].

The observed mutually exclusive expression of Ret and Met by the two lineages of enteric neurons in the mature adult ENS is consistent with an earlier study that reported that a deletion of Met in the Wnt1-cre expressing NC-lineage did not alter the abundance of MET^{+} neurons in the adult ENS[41]. In this study, we also show that MENs are dependent on HGF-MET signaling in a manner analogous to the requirement of GDNF-RET signaling by NENs. Further, Ret haploinsufficiency-mediated loss of the NEN lineage causes a proportional increase in the MEN lineage. This suggests the presence of yet unknown quorum sensing signaling mechanisms between the two lineages that reciprocally regulate their populations to maintain the structure of the post-natal ENS. This also implies the existence of a precursor cell responsible for the expansion of the MEN population in a manner analogous to what we have previously described for NENs[71].

The validation of mesodermal markers (MHCst and MET) in a subset of adult human ENS neurons suggests that our findings may be of clinical importance. The loss of NENs and the corresponding dominance of MENs begins in early adulthood and maybe viewed as part of the normal maturation of the ENS. However, because of its progressive nature, it may have pathological implications for the elderly gut. Many gastrointestinal motility functions are compromised with advancing age, resulting in clinically significant disorders[72]. A progressive imbalance in these two populations in favor of MENs with age may therefore have functional consequences. Although the exact mechanisms will need to be worked out, our results indicate that a MENs-predominant ENS is associated with significant differences in gut motility. Understanding the forces that regulate parity between these two different sources of neurogenesis therefore holds the promise of arresting or reverting progressive loss of gut motility with increasing age. Our results may also have implications for the pathogenesis of disordered motility unrelated to aging, as downregulation of Gdnf and Ret expression has been associated with diverticular disease and obstructed defecation

in adult patients[57,73,74]. GWAS analyses further showed that Gdnf gene was in the eQTL associated with increased incidence of diverticular disease[75]. It is in this context that the identification of SNAP-25 as a NENs marker gene and the transcriptomic pattern analyses of patients with chronic obstructed defecation are significant. Expression of Snap25 is upregulated by GDNF and is significantly downregulated in gut tissues of patients with diseases associated with significant reduction in GDNF-RET signaling (diverticular disease and obstructed defecation)[48,57,73]. Thus, while earlier thought to be a pan-neuronal marker[46,76], establishing the identity of SNAP-25 as a NEN lineage-restricted marker provides us not only with an important tool to query proportions of NENs in murine and human tissue but also suggests the NENs-limited nature of prior observations based on Snap25 transgenic animals[76,77]. Gut dysmotility disorders that present with conserved ENS neuronal numbers[73] have puzzled investigators on the etiology of the disease. Our results suggest an explanation based on NENs-to-MENs lineage shifts that conserve overall enteric neuronal numbers with variable effects on function.

In conclusion, the ENS of the juvenile and mature mammalian gut is dominated by two different classes of neurons that have distinct ontogenies and trophic factors, associated with functional differences. The shift in neuronal lineage may represent a functional adaptation to changes in nutrient handling, microbiota or other physiological factors associated with different ages. Further research in the regulation of the parity between these two nervous systems in humans during the lifetime will be important to advance our understanding of the adult ENS and the treatment of age-related and other pathological disorders of gut motility.

Acknowledgements

We would like to thank Dr. Chulan Kwon (JHU) for his kind gift of the Mesp1-cre mice, Dr. Jeremy Nathans (JHU) for his kind gift of the Tek-EGFP, Tek-cre and *Hprt*-tdTomato lineage-traced mice and his support, and Dr. Vanda Lennon (Mayo Clinic) for her kind gift of the ANNA1 anti-Hu antisera. We thank Dr. Xinzhong Dong (JHU) and Dr. Mark Donowitz (JHU) for their support. The microscopy was performed on the Ross Imaging Core at the Hopkins Conte Digestive Disease Center at the Johns Hopkins University (P30DK089502) using the Olympus FV 3000rs (procured with the NIH-NIDDK S10 OD025244 grant) and we thank Dr. George McNamarra for his help with confocal training and imaging. The 10X Genomics Chromium processing for scRNAseq was performed at the GRCF Core and the sequencing was performed at the CIDR core at the Johns Hopkins University. S.K. was funded through a grant from the Ludwig Foundation, a grant from the NIA (R01AG066768), a pilot award from the Hopkins Digestive Diseases Basic & Translational Research Core Center grant (P30DK089502). L.A.G was funded in part by a Johns Hopkins Catalyst Award and a grant from the NIA (R01AG066768). P.J.P. was funded through the Hopkins Conte Digestive Disease Center at the Johns Hopkins University (P30DK089502), NIDDK (R01DK080920), the Maryland Stem Cell Research Foundation (MSCRF130005), and a grant from the AMOS family.

Author contributions

S.K., and P.J.P. conceived the study; S.K., M.A., M.L, L.A.G. and P.J.P. designed the research studies; S.K. L.B, C.Z, A.S., A.B., and M.S. conducted the experiments; S.K., Z.H., M.K., J.L., L.B., S.B., E.V., J.S., S.N., M.S., G.L., and L.A.G. acquired and analyzed the data; S.K., and P.J.P drafted the manuscript.

Methods

Animals:

Experimental protocols were approved by The Johns Hopkins University's Animal Care and Use Committee in accordance with the guidelines provided by the National Institutes of Health. Presence of vaginal plug was ascertained as 0.5 days post-fertilization and this metric was used to calculate age of mice. Only male mice were used for the studies detailed in this report. The Wnt1-cre:*Rosa26*-tdTomato lineage-traced line was generated as detailed before by breeding the B6.Cg-Tg(*Wnt1-cre*) with the Ai14 transgenic mouse line (Jax #: 007914) containing the *Rosa26*-tdTomato transgene[71,78,79]. Pax3-cre:*Rosa26*-tdTomato lineage-traced line was generated by breeding the Ai9 transgenic mouse line (Jax #: 007909) with the Pax3-cre transgenic mouse (Jax #: 005549). The Wnt1-cre:*Hprt*-tdTomato mouse was generated by breeding our aforementioned Wnt1-cre transgenic mouse line with the *Hprt*-tdTomato transgenic mouse line (Jax #: 021428, kind gift from Prof. Jeremy Nathans). Mesp1-cre:*Rosa26*-tdTomato mice were generated by breeding the Mesp1-cre transgenic mice[80] (gift from Dr. Chulan Kwon, JHU) with the Ai14 transgenic mice. $Ret^{+/CFP}$ mice (MGI:3777556) were inter-bred to get a colony of adult $Ret^{+/+}$ and $Ret^{+/CFP}$ mice. $Ret^{CFP/CFP}$ mice died at or before term. Tek-cre:*Hprt*-tdTomato mice were generated by breeding Tek-cre transgenic mice (also known as Tie2-cre; Jax #: 004128) with the *Hprt*-tdTomato transgenic mouse line. 17-month-old male C57BL/6 mice from the aging mouse colony of the National Institute of Aging were procured for the GDNF-treatment experiment.

Human Tissues:

Human tissues were obtained under IRB protocol IRB00181108 that was approved by Institutional Review Board at the Johns Hopkins University. Pathological normal specimens of human duodenum and colon were obtained post-resection. Tissues were obtained from adult donors and were de-identified such that the exact age, gender, and ethnicity of the donors was unknown.

Tissue preparation:

Mice were anesthetized with isoflurane and sacrificed by cervical dislocation. A laparotomy was performed, and the ileum was removed and lavaged with PBS containing penicillin-streptomycin (PS; Invitrogen), then cut into 1-cm-long segments and placed over a sterile plastic rod. A superficial longitudinal incision was made along the serosal surface and the LM-MP was peeled off from the underlying tissue using a wet sterile cotton swab [71] and placed in Opti-MEM medium (Invitrogen) containing Pen-Strep (Invitrogen). The tissue was then laid flat and fixed with freshly prepared ice cold 4% paraformaldehyde (PFA) solution for 45 minutes in the dark to preserve fluorescence intensity and prevent photo-bleaching. After the fixation, the tissue was removed and stored in ice cold sterile PBS with Pen-Strep for immunofluorescence staining and subsequent microscopy.

For human tissues, duodenal tissue from adult human patients (n = 3 patients), who did not have any prior history of chronic intestinal dysmotility, that was removed by Whipple procedure was obtained. A colonic sample from a pathologically normal colonic resection from an adult donor suffering from colon carcinoma who similarly did not have prior history of chronic intestinal dysmotility was also obtained. The resected tissue was placed in ice cold Opti-MEM medium (Invitrogen) containing Pen-Strep (Invitrogen). The mucosal and sub-mucosal tissue was dissected out in the medium under light microscope and the muscularis layer containing myenteric plexus tissue was obtained. The tissue was laid out between two glass slides and fixed overnight in ice cold 4% PFA after which it was removed and stored in ice cold sterile PBS with Pen-Strep for immunofluorescence staining, optical clarification and subsequent microscopy.

Immunohistochemistry:

For murine tissue: The fixed LM-MP tissue was washed twice in ice-cold PBS in the dark at 16 °C. The tissue was then incubated in blocking-permeabilizing buffer (BPB; 5% normal goat serum

with 0.3% Triton-X) for 1 hour. While staining for antibodies that were mouse monoclonal, 5% normal mouse serum was added to the BPB. The tissue was then removed from the BPB and was incubated with the appropriate primary antibody at the listed concentration (Table S1) for 48 h at 16 °C in the dark with shaking at 55 rpm. Following incubation with primary antibody, the tissue was washed three times (15-min wash each) in PBS at room temperature in the dark. The tissue was then incubated in the appropriate secondary antibody at room temperature for 1 hour while on a rotary shaker (65 rpm). The tissue was again washed three times in PBS at room temperature, counterstained with DAPI to stain the nuclei, overlaid with Prolong Antifade Gold mounting medium, cover-slipped, and imaged.

Colchicine treatment: For CGRP immunostaining, mice were injected with Colchicine at a concentration of 5 mg/Kg body weight 16 hours (overnight) before they were sacrificed. The mice were housed singly during this time and adequate gel packs were provided. Food and water were provided *ad libitum*. On the following day, the mice were sacrificed, and their LM-MP tissues were harvested as detailed above.

For human tissue: The fixed muscularis layer containing myenteric plexus tissue was removed from ice cold PBS and incubated in blocking-permeabilizing buffer (BPB; 5% normal goat serum, 5% normal mouse serum with 0.3% Triton-X) for 4 hours. The tissue was then removed from the BPB and was incubated with the appropriate primary antibody at the listed concentration (Table S1) for 5 days at 16°C in the dark with shaking at 55 rpm. Following incubation with primary antibody, the tissue was washed five times (15-min wash each) in PBS at room temperature in the dark. The tissue was then incubated in the appropriate secondary antibody at 16°C in the dark with shaking at 55 rpm for 2 days. The tissue was again washed in dark for five times in PBS that contained DAPI at room temperature. After the final wash, the tissue was suspended in tissue clarification buffer CUBIC[81] for 1 hour at 4°C in the dark after which it was overlaid with Prolong Antifade Gold mounting medium, cover-slipped, and imaged. Briefly, the CUBIC optical

clarification buffer was made by mixing 2.5 g of urea (25% by wt), 2.5 g of N, N, N´, N´-tetrakis (2-hydroxy-propyl) ethylenediamine (25% by wt), 1.5 g of Triton X-100 (15% by wt) in 35 ml of Distilled Water. The solution was shaken till the ingredients were dissolved and yielded a clear viscous solution.

Microscopy:

Imaging was done by using the oil immersion 63X objective on the Leica SP8 confocal microscope and by using the oil immersion 40X objective on the Olympus Fluoview 3000rs confocal microscope with resonance scanning mode. For thick tissues, such as human tissues, the Galvano mode of the Olympus Fluoview 3000rs microscope that enabled higher resolution imaging and averaging was used. Images obtained were then analyzed using Fiji (https://fiji.sc/).

Enumeration of neurons:

Identification of myenteric ganglia was performed according to our pre-determined method published earlier[71]. Briefly, contiguous clusters of neurons were defined as a ganglia and the total numbers of neurons within these clusters were enumerated as numbers of myenteric neurons per ganglion. As a rule, clusters of 3 neurons or more were deemed to consist a ganglion and our enumeration strategy did not count extra-ganglionic neurons. We imaged atleast 10 ganglia per tissue for our enumeration and each group studied had $n \geq 3$ mice. Identification and enumeration of neurons and detection of co-localization was performed manually by trained laboratory personnel.

Protein isolation and detection:

After the LM-MP tissue was isolated, it was weighed and placed in a sterile 1.5 ml microfuge tube. 1X RIPA buffer (Cell Signaling Technology) with Halt Protease Inhibitor Cocktail (Thermo Scientific) at 5X concentration, Phosphatase Inhibitor Cocktails II and III (Sigma-Aldrich) at 2X concentrations were added to the tissue lysate buffer. Tissue was disrupted using 1.0 mm silica

beads in Bullet Blender 24 (Next Advance) for 5 mins at highest setting. The lysate was incubated at 4°C with shaking for 30 mins, centrifuged at 14,000rpm for 20 mins and the supernatant was taken and stored in -80°C in aliquots. Protein concentration was estimated using Bradford assay solution (Biorad) following the manufacturer's protocol. For immunoblotting, 40 µg of protein was loaded per well of 4%-20% gradient denaturing gel (Biorad). Protein marker used was Precision Plus Dual Color standards (Biorad). After fractionating the proteins, they were blotted onto ImmunBlot PVDF membrane (Biorad) overnight at 4°C at 17V for 12-16 hours. After blotting, membrane was blocked with Odyssey TBS blocking buffer (Li-Cor) for 1 hour at room temperature with shaking. Incubation with primary antibodies were carried out at 4°C with shaking for 24 hours. Following binding, the blot was washed 4 times with TBS-T (Tris Buffered Saline with 0.5% Tween) for 15 mins each with shaking at room temperature. Secondary antibody incubation was carried out in dark at room temperature for 1.5 hours with shaking. The blot was then washed 4 times for 15 mins each and imaged on Odyssey CLx system (Li-Cor). Antibodies used are detailed in the Table S1.

RNA isolation and quantitative detection of specific transcripts:

The isolated tissue was stored in RNALater Solution (Ambion). RNA was isolated using RNeasy Mini Kit (Qiagen) following manufacturer's protocol. RNA quantification was carried out using Epoch Microplate Spectrophotometer (BioTek). cDNA synthesis was carried by SuperScript IV VILO Master Mix (Invitrogen). Quantitative Real-time PCR was carried out using Taqman Gene Expression Master Mix (Applied Biosystems) and Roto-Gene Q (Qiagen). The probes used are listed in Table S1.

Single Cell RNA sequencing and analyses:

Single cell preparation from adult murine ileal tissues: Ileal tissues from two 6-month old adult male littermate C57/BL6 wildtype mice were isolated by peeling as previously described. The

tissues were then dissociated in Digestion Buffer containing 1 mg/ml Liberase (Sigma-Aldrich) in OptiMEM. Tissues from mouse 1 were dissociated in the Digestion buffer containing Liberase TH and tissues from mouse 2 were dissociated in the Digestion buffer containing Liberase TL. Dissociation was performed at 37°C for 30 minutes on a rotary shaker, after which the cells were centrifuged at 200g for 7 minutes, and the pellet was resuspended in ice cold sterile PBS. The cell suspension was passed through a 40 µm cell sieve and the resulting filtered cell suspension was again centrifuged at 200g for 7 minutes. This process of cell centrifugation and filtration was repeated two more times, after which the cells were resuspended in 1 ml ice cold sterile PBS. The repeated steps of serial cell washes and filtration removed clumps and debris and the viability of the resulting cell suspension was estimated to be >90% using Trypan Blue dye test. The cells were then processed through 10X Genomics Chromium V2.0 system according to the manufacturer's suggested workflow. The processing was done at the GRCF Core Facility at the Johns Hopkins University. The pooled libraries were sequenced on an Illumina HiSeq 2500 to an average depth of 3.125×10^8 reads per sample library. The sequencing was performed at the CIDR core facility at the Johns Hopkins University.

Pre-processing of FASTQs to Expression Matrices: FASTQ sequence files were processed following a Kallisto Bustools workflow compatible with downstream RNA velocity calculations [kallisto == 0.46.1, bustools == 0.39.3][82]. References required for pseudo-alignment of transcripts were obtained using the get_velocity_files (functionality of BUSpaRSE (https://github.com/BUStools/BUSpaRse)), with "L=98" for 10X Genomics v2.0 sequencing chemistry. Reads were pseudo-aligned to an index built from Ensembl 97 transcriptome annotation (Gencode vM22; GRCm38). Across two samples processed, a total of 578,529,125 reads were successfully pseudo-aligned. Barcodes within a Hamming distance of one to known 10X Genomics v2.0 barcodes were corrected. Reads were classified as "spliced" or "unspliced" by their complement to the target list of intronic sequences and exonic sequences, respectively,

and subsequently quantified separately into expression count matrices. Spliced counts are used for all analyses.

Single cell gene expression analysis: scRNA-seq count matrices were analyzed using Monocle3. 11,123 high-quality cells were identified as meeting a 200 UMI minimum threshold with a mitochondrial read ratio of less than 20%; droplets that did not meet these criteria were excluded from the analysis. Mitochondrial counts were determined as the sum of reads mapping to 37 genes annotated to the mitochondrial genome. All genes with non-zero expression were included for downstream analysis. Raw counts were first scaled by a cell-size scaling factor and subsequently log10 transformed with a pseudo-count of 1. Normalized values are used in place of raw counts unless otherwise noted.

Prior to UMAP dimensionality reduction, batch effects between the two biological replicates were assessed and corrected via the mutual nearest neighbors (MNN) algorithm as implemented by Batchelor in Monocle3 (50 principal components, with default k=20) [83]. 15 clusters of cells in the UMAP embedding were identified by Leiden community detection (resolution = 1e -5, number of iterations = 5). 30 marker genes for each cluster were identified based on greatest pseudo R^2 values and used for supervised annotation of cell types by searching UniProt, Allen Cell Atlas and through literature search with Pubmed.

NC-derived cell clusters were identified by expression of NC markers Ret and Sox10. MEN cluster was identified by its expression of CGRP-coding Calcb, Met, and Cdh3. The pan-MENs protein marker MHCst was identified by labeling with an antibody S46 which labels all members of the MHCst family[38]. Since the antibody does not identify a single gene product, MHCst immunostaining could not be used to identify a specific gene marker for use in the annotation of the MEN cluster. For further analysis into the MENs population, the full LM-MP dataset was subset to include only the 2,223 cells annotated as such. These cells were re-processed as above, but with a reduced PCA dimensionality of k=20 as input for the UMAP embedding. 5 clusters of cells

in the UMAP embedding were identified by Leiden community detection (k= 10, resolution = 5e -4). The two samples showed a similar distribution of cells across the various cell clusters (Fig S3A). The MEN cluster had a significantly higher mean UMI count/cell compared to the NC-derived cell cluster (Mean UMI ± S.E.M. of UMI/cell: MENs: 4045.6 ± 113.4; NENs: 1247.9 ± 38.9; $t = 23.34$, $df = 2727.8$, $p < 2.2e-16$; Welch two sample t-test; Fig S4D). Total UMI per cell is correlated directly with cell size[84]. A significantly higher UMI/cell in MENs compared to NENs suggests that MENs would have significantly larger cell size compared to NENs, which we have confirmed in Fig S4A.

Pattern discovery and ProjectR analyses: Pattern discovery was utilized to identify sets of co-expressed genes that define cell-type specific transcriptional signatures. The normalized expression matrix was decomposed via non-negative matrix factorization (NMF) as implemented in the R package *NNLM* (https://github.com/linxihui/NNLM), with k=50 and default parameters. Cell weights for each pattern were grouped by assigned cell-type and represented by heatmap. Pattern vectors were hierarchically clustered by a Euclidian distance metric, implemented in ComplexHeatmap (https://github.com/jokergoo/ComplexHeatmap)[85]. These patterns were then tested on the bulk RNA-Seq expression matrix for the Human Obstructed Defecation study[57] (GSE101968). The log2 expression (log2(rpkm + 1)) from this study was projected onto the NMF patterns using projectR[61]. Students' t tests were performed on the projection weights from the Control and OD groups to test for differences between them.

Whole gut transit time analyses:

Whole-gut transit time (WGTT) for every mouse was analyzed by the method using the carmine red protocol[71]. Mice were placed in individual cages and deprived of food for 1 hour before receiving 0.3 mL 6% (wt/vol) carmine solution in 0.5% methylcellulose by oral gavage into the animal's stomach. The time taken for each mouse to produce a red fecal pellet after the administration of carmine dye was recorded in minutes. The experiment was terminated at 210

minutes post-gavage and the WGTT of any mice that did not expel the red dye at the termination was marked at the value of 210 min. The mean difference in whole gut transit time (in minutes) between both the $Ret^{+/+}$ and $Ret^{+/-}$ mice cohorts, and the GDNF and Saline-treated Control cohorts were analyzed statistically.

In vivo Injections:

GDNF injection: Similar to prior report that gave sub-cutaneous injections of GDNF to post-natal mice[54], we took 6 littermate 10 day old (P10) male Wnt1-cre:*Rosa26*-tdTomato mice and divided into two subgroups, GDNF and Control. Each mouse in the GDNF group was injected sub-cutaneously with 50 µl of 2mg/ml of GDNF (Peprotech Catalogue #: 450-44) every other day, while the Control group was injected with 50 µl of sterile saline. The mice were given 5 doses and then sacrificed on P20, after which their LM-MP tissues were isolated as detailed above. The tissues were then immunostained with antibodies against HuC/D and imaged. In a separate experiment, adult (P60) mice were also injected sub-cutaneously with GDNF (100 µl of 100 µg/ml of GDNF). The mice were given 5 doses over a course of 10 days and then sacrificed on P70, after which their LM-MP tissues were isolated as detailed above. For studying the effect of GDNF on aging mice, two cohorts of 17-month-old male C57BL/6 mice (n=5 mice/cohort) were obtained from the aging colony of the National Institute of Aging. Before the start of dosing, the whole gut transit time was assayed. The animals were then injected daily sub-cutaneously either with 100 µl of saline (Control) or 100 µl of GDNF (500 µg/ml) for 10 consecutive days, after which the mice were sacrificed and their LM-MP tissues were isolated as detailed above. The tissues were then immunostained with antibodies against HuC/D and imaged.

HGF injection: Similar to prior report that gave sub-cutaneous injections of HGF to post-natal mice, we took 6 littermate 10 day old (P10) male Wnt1-cre:*Rosa26*-tdTomato mice and divided into two subgroups, HGF and Control. Each mouse in the HGF group was injected sub-

cutaneously with 100 µl of 2mg/ml of HGF (Peprotech Catalogue #:315-23) every other day, while the saline group was injected with 100 µl of sterile saline. The mice were given 5 doses and then sacrificed on P20, after which their LM-MP tissues were isolated as detailed above. The tissues were then immunostained with antibodies against HuC/D and imaged.

Statistics:

Data was analyzed using Graphpad Prism 8.3.1 and R using Unpaired Students t-test, Simple Linear Regression, and Ordinary One-Way ANOVA.

Data:

All raw data are provided in Supplementary Table 2-22. We imaged atleast 10 ganglia per tissue for our enumeration and each group studied had n ≥ 3 mice. Raw single cell RNA sequencing data is archived on the NCBI GEO server and can be accessed under the accession number GSE156146.

Figures

Fig 1: Half of all adult small intestinal myenteric neurons are derived from a non-neural crest lineage.

(A) Enteric glia, labeled with GFAP (green) in the myenteric plexus from an adult Wnt1-cre:*Rosa26*-tdTomato mouse. Inset is magnified in color segregated panels, showing $GFAP^+$ glia co-expressing tdTomato (red, red arrows). Nuclei are labeled with DAPI (blue). Scale bar = 10 µm.

(B) Enteric neurons, labeled with HuC/D (green) in the myenteric plexus from an adult Wnt1-cre:*Rosa26*-tdTomato mouse. Inset is magnified in color segregated panels, showing only a subpopulation of neurons co-express tdTomato (red arrows) while many neurons do not (white arrows). Nuclei are labeled with DAPI (blue). Scale bar = 10 µm.

(C) Quantification of $tdTomato^+$ and $tdTomato^-$ neurons in the myenteric ganglia of P60 Wnt1-cre:*Rosa26*-tdTomato mice show equal proportions of both neuronal types.

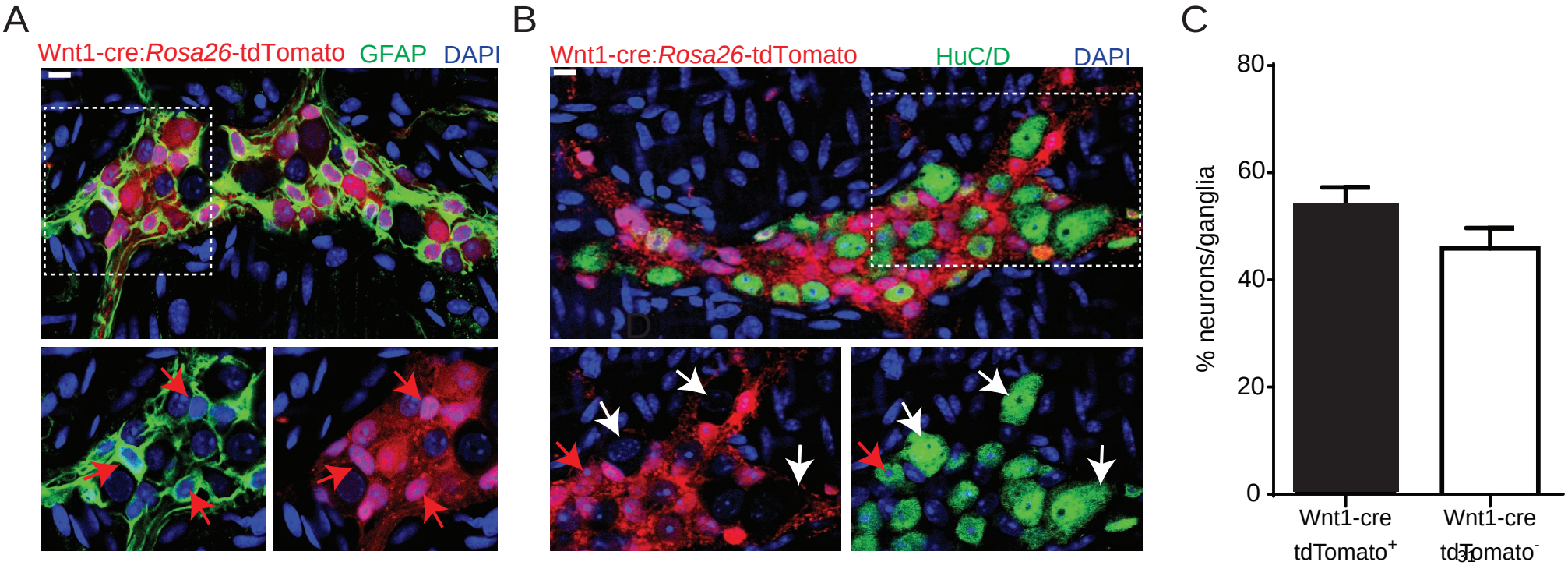
A
Wnt1-cre:Rosa26-tdTomato
GFAP
DAPI
B
Wnt1-cre:Rosa26-tdTomato
HuC/D
DAPI
C
% neurons/ganglia
80
60
40
20
0
Wnt1-cre tdTomato+
Wnt1-cre tdTomato-

Figure 1

Fig 2: Mesoderm-lineage-tracing and marker expression provide evidence of the mesodermal-derivation of half of all adult small intestinal myenteric neurons.

(A) Small intestinal LM-MP from adult male Tek-cre:*Hprt*-tdTomato shows the presence of Tek-derived and hence mesoderm-derived tdTomato^{+} (red) HuC/D^{+} (green) neurons (white arrows) and non-mesoderm-derived tdTomato^{-} neurons (green arrows). Vascular cells depict higher fluorescence intensity (yellow arrow) than cells in the ganglia. Nuclei are labeled with DAPI. Scale bar = 10 µm.

Cardiac and small intestinal tissues from (B) heart and (C) small intestinal LM-MP layer of adult male Mesp1-cre:*Rosa26*-tdTomato mice shows the presence of variable tdTomato expression in cells of these tissues. While cardiomyocytes in heart and cells within the myenteric ganglia (white arrows) exhibit lower tdTomato fluorescence, similar to the tissues from Tek-cre:*Hprt*-tdTomato mice in (A), the vascular cells exhibit higher fluorescence intensity (yellow arrows). Scale bar = 10 µm.

(D) Small intestinal LM-MP from adult male Mesp1-cre:*Rosa26*-tdTomato shows the presence of mesoderm-derived tdTomato^{+} (red) HuC/D^{+} (green) neurons (white arrows) and non-mesoderm-derived tdTomato^{-} neurons (green arrows). Nuclei are labeled with DAPI. Scale bar = 10 µm.

(E) Quantification of tdTomato-expressing and non-expressing neurons in the myenteric ganglia of P60 Mesp1-cre:*Rosa26*-tdTomato mice.

MHCst immunolabeling exclusively marks all the (F) mesoderm-derived adult HuC/D^{+} (green) neurons in the small intestinal LM-MP of Mesp1-cre:*Rosa26*-tdTomato mice; and (G) all the non-NC-derived neurons in the small intestinal LM-MP of Wnt1-cre:*Rosa26*-tdTomato mice (white

arrows). MHCst does not label tdTomato^{+} NC-derived cells (yellow arrows). Nuclei are stained with DAPI (blue). Scale bar = 10 µm.

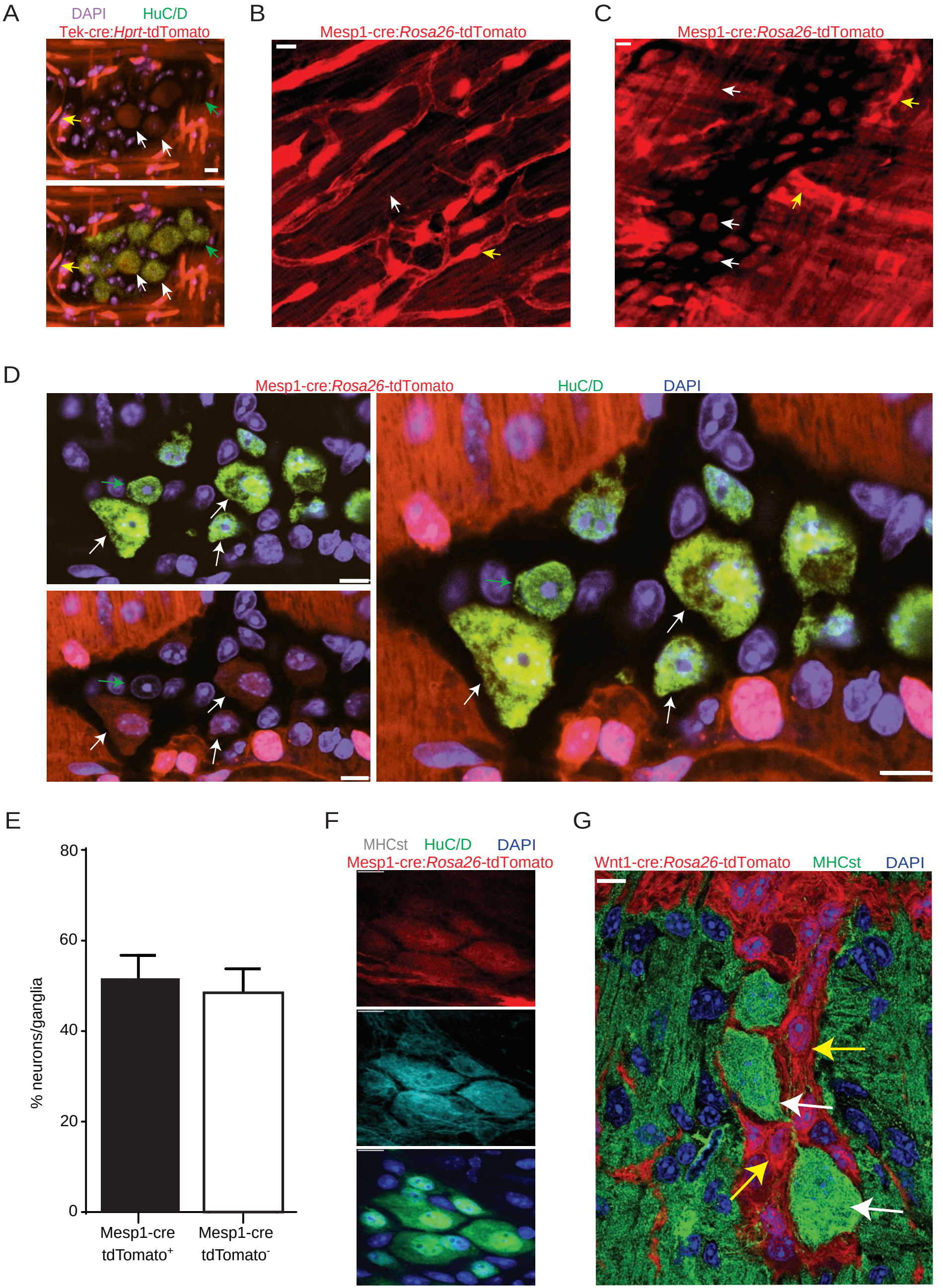
A
DAPI
HuC/D
Tek-cre:Hprt-tdTomato
B
Mesp1-cre:Rosa26-tdTomato
C
Mesp1-cre:Rosa26-tdTomato
D
Mesp1-cre:Rosa26-tdTomato
HuC/D
DAPI
E
% neurons/ganglia
80
60
40
20
0
Mesp1-cre tdTomato+
Mesp1-cre tdTomato-
F
MHCst
HuC/D
DAPI
Mesp1-cre:Rosa26-tdTomato
G
Wnt1-cre:Rosa26-tdTomato
MHCst
DAPI

Figure 2

Fig 3: Cellular and molecular phenotyping of MENs and NENs.

MET immunostaining (green) labels (A) Wnt1-cre:*Rosa26*-tdTomato^{-} MENs and (B) a population of Mesp1-cre:*Rosa26*-tdTomato^{+} MENs (white arrow) while not labeling all MENs (red arrow).

(C) RET immunostaining (green) only labels Wnt1-cre:*Rosa26*-tdTomato^{+} NENs (green arrow) and not tdTomato^{-} MENs (white arrows).

(D) NOS1 is expressed by both tdTomato^{+} NENs (red, white arrows) and tdTomato^{-} MENs (blue arrows) in an adult Wnt1-cre:*Rosa26*-tdTomato mouse, but most MENs do not express NOS1 (marked by *).

(E) NEN lineage contains significantly higher proportions of NOS1^{+} neurons compared to MEN lineage in Wnt1-cre:*Rosa26*-tdTomato mice. Data represent mean ± S.E.M. (**** $p < 0.0001$).

(F) Both tdTomato^{+} (red) and tdTomato^{-} neurons in the myenteric plexus of an adult Wnt1-cre:*Rosa26*-tdTomato mouse (HuC/D, green) express CGRP (blue) Inset showing a tdTomato^{-} CGRP^{+} neuron (white arrow) is magnified on the right.

(G) MEN lineage contains significantly higher proportions of CGRP^{+} neurons compared to NEN lineage in Wnt1-cre:*Rosa26*-tdTomato male mice. Data represent mean ± S.E.M. (*** $p < 0.001$).

(H) MENs express the protein P-Cadherin/CDH-3 (green; white arrows) while tdTomato^{+} (red) NENs do not (blue arrows) in myenteric ganglia from adult Wnt1-cre:*Rosa26*-tdTomato mice.

Nuclei in (B), (C), (H) are labeled with DAPI (blue). Scale bar for all images denotes 10 µm.

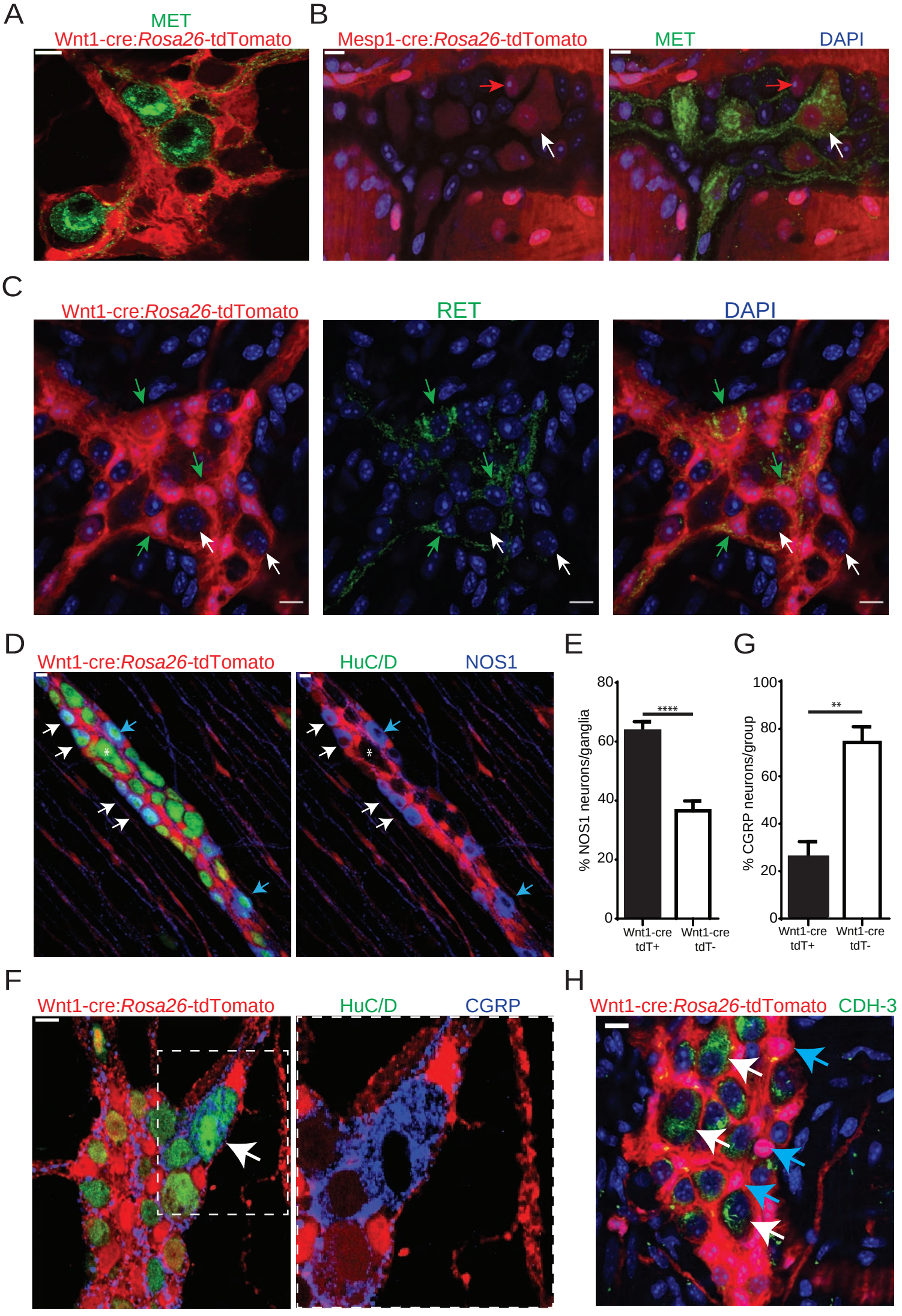
A
MET
Wnt1-cre:Rosa26-tdTomato
B
Mesp1-cre:Rosa26-tdTomato
MET
DAPI
C
Wnt1-cre:Rosa26-tdTomato
RET
DAPI
D
Wnt1-cre:Rosa26-tdTomato
HuC/D
NOS1
E
% NOS1 neurons/ganglia
80
60
40
20
0
****
Wnt1-cre tdT+
Wnt1-cre tdT-
G
% CGRP neurons/group
100
80
60
40
20
0
**
Wnt1-cre tdT+
Wnt1-cre tdT-
F
Wnt1-cre:Rosa26-tdTomato
HuC/D
CGRP
H
Wnt1-cre:Rosa26-tdTomato
CDH-3

Figure 3

Fig 4: scRNAseq-analyses identifies the distinct transcriptomic profile of the MENs.

(A) UMAP representation of 11,123 sequenced high-quality cells that were identified as meeting a 200 UMI minimum threshold with a mitochondrial read ratio of less than 20%. Clusters were annotated by markers that were found to be cell-type specific by searching UniProt, Allen Cell Atlas and Pubmed databases. Cells of the neural crest lineage were then identified as NC-cells by co-expression of neural crest marker genes Ret and Sox10, or as MENs by co-expression of Calcb (CGRP), Cdh3, and Met genes.

(B) Cluster-specific expression patterns of select markers.

(C) Validation of the MENs-specific marker genes discovered in the scRNAseq analyses by immunohistochemistry and confocal microscopy of small intestinal LM-MP from adult male Wnt1-cre:*Rosa26*-tdTomato mice. Immunostaining of the proteins AEBP1, CFTR, CLIC3, FMO2, NT3, SLPI, SMO, MYL7, IL-18, SLC17A9, and CDH3 (green; green arrows) was found to be localized to tdTomato^{-} MENs. tdTomato^{+} (red) NC-cells did not immunostain for these markers (red arrows). Nuclei were labeled with DAPI (blue). Scale bar denotes 10 µm.

A

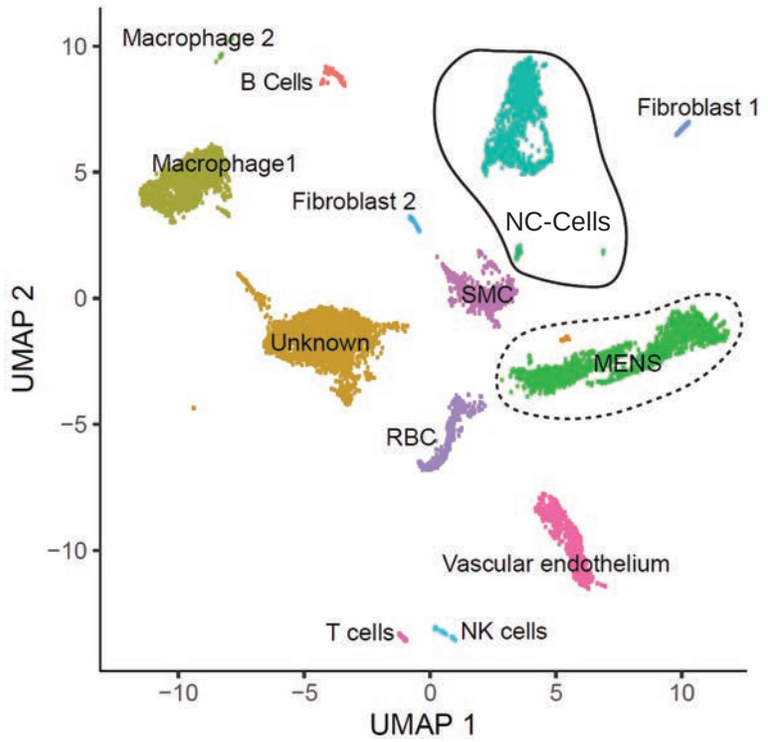
Macrophage 2
B Cells
Macrophage1
Fibroblast 2
Fibroblast 1
NC-Cells
SMC
Unknown
MENS
RBC
Vascular endothelium
T cells
NK cells
UMAP 2
UMAP 1
10
5
0
−5
−10

B

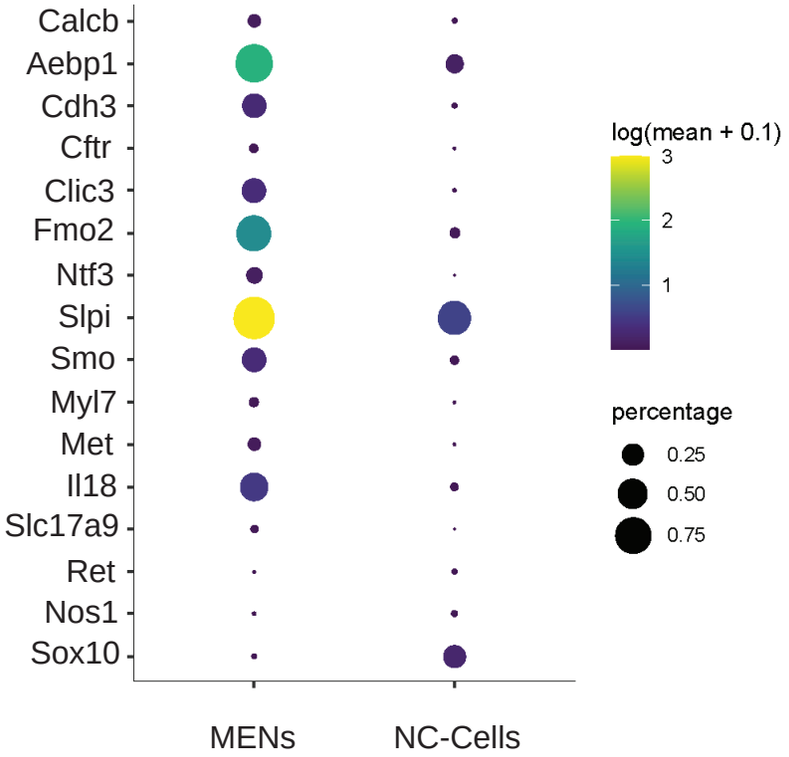
Calcb
Aebp1
Cdh3
Cftr
Clic3
Fmo2
Ntf3
Slpi
Smo
Myl7
Met
Il18
Slc17a9
Ret
Nos1
Sox10
MENs
NC-Cells
log(mean + 0.1)
3
2
1
percentage
0.25
0.50
0.75

C

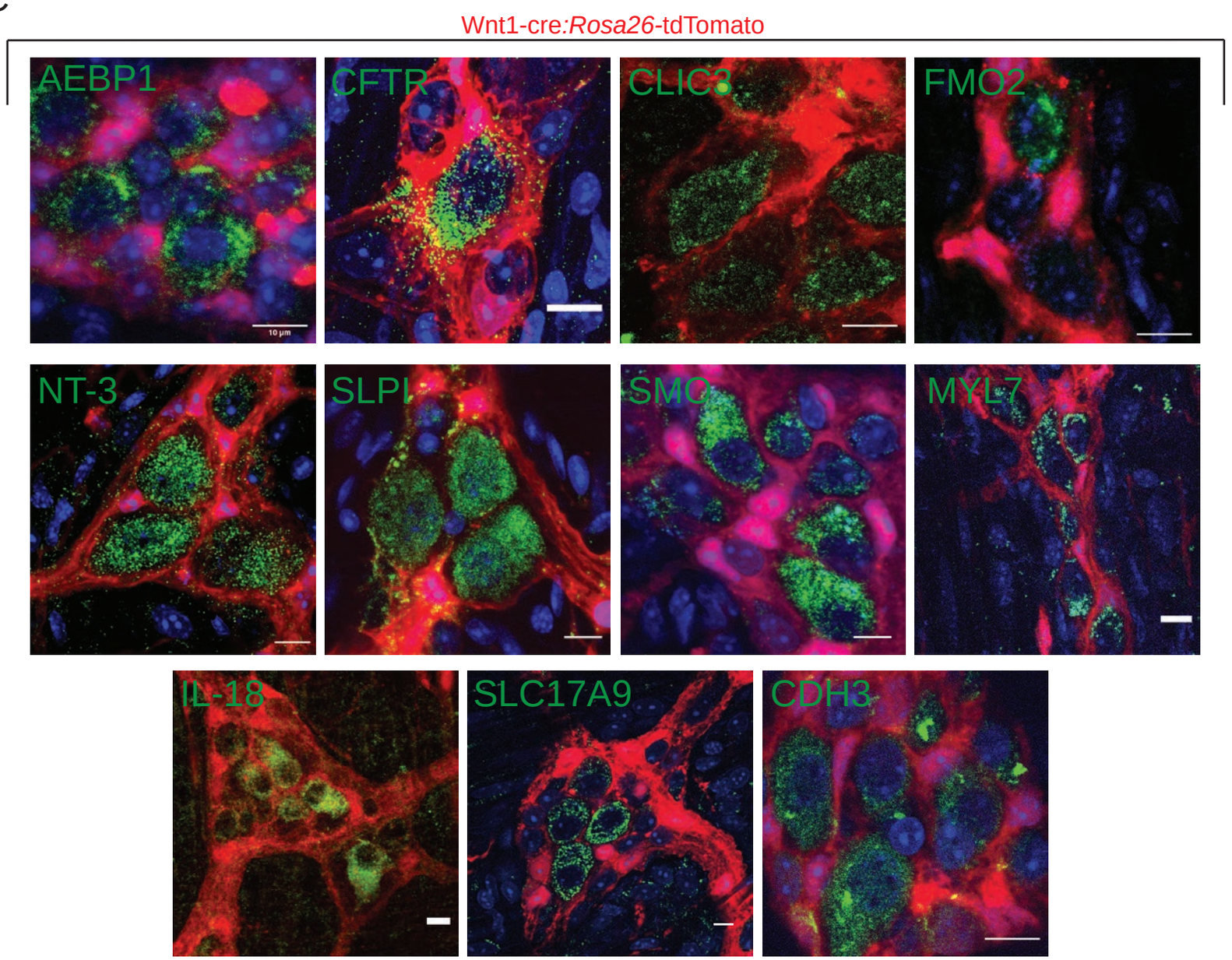
Wnt1-cre:Rosa26-tdTomato
AEBP1
CFTR
CLIC3
FMO2
NT-3
SLPI
SMO
MYL7
IL-18
SLC17A9
CDH3

Figure 4

Fig 5: SNAP-25 expression is restricted to the neural crest lineage in the adult myenteric ganglia.

SNAP-25 expression (green) co-localizes with tdTomato (red) but not with the MENs marker MHCst (cyan) as observed in (A) 2D and (B) orthogonal views of a myenteric ganglia from a Wnt1-cre:*Rosa26*-tdTomato mouse that was immunolabeled with antibodies against MHCst and SNAP-25. Nuclei were labeled with DAPI (blue). Scale bar denotes 10 µm.

A

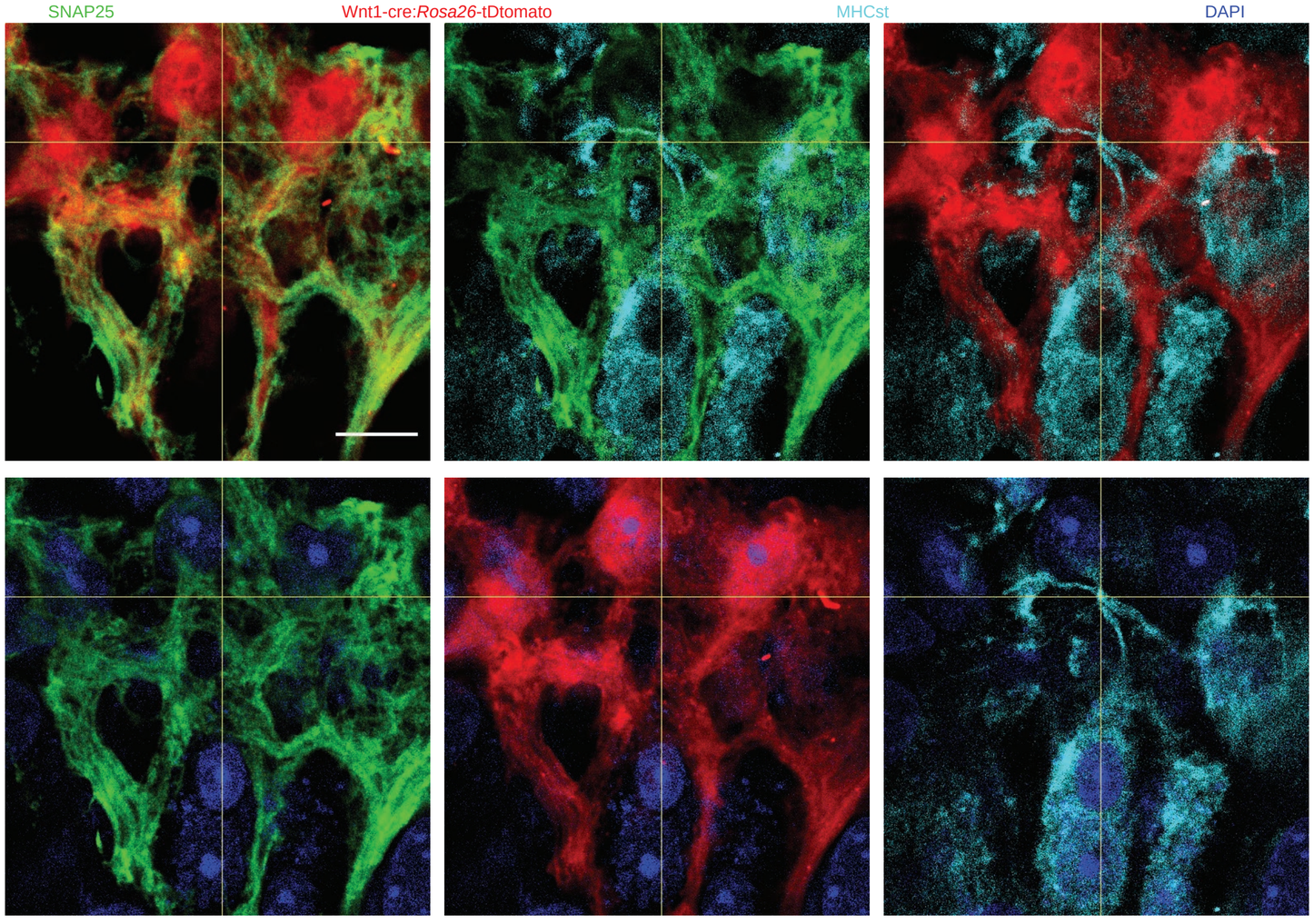

B

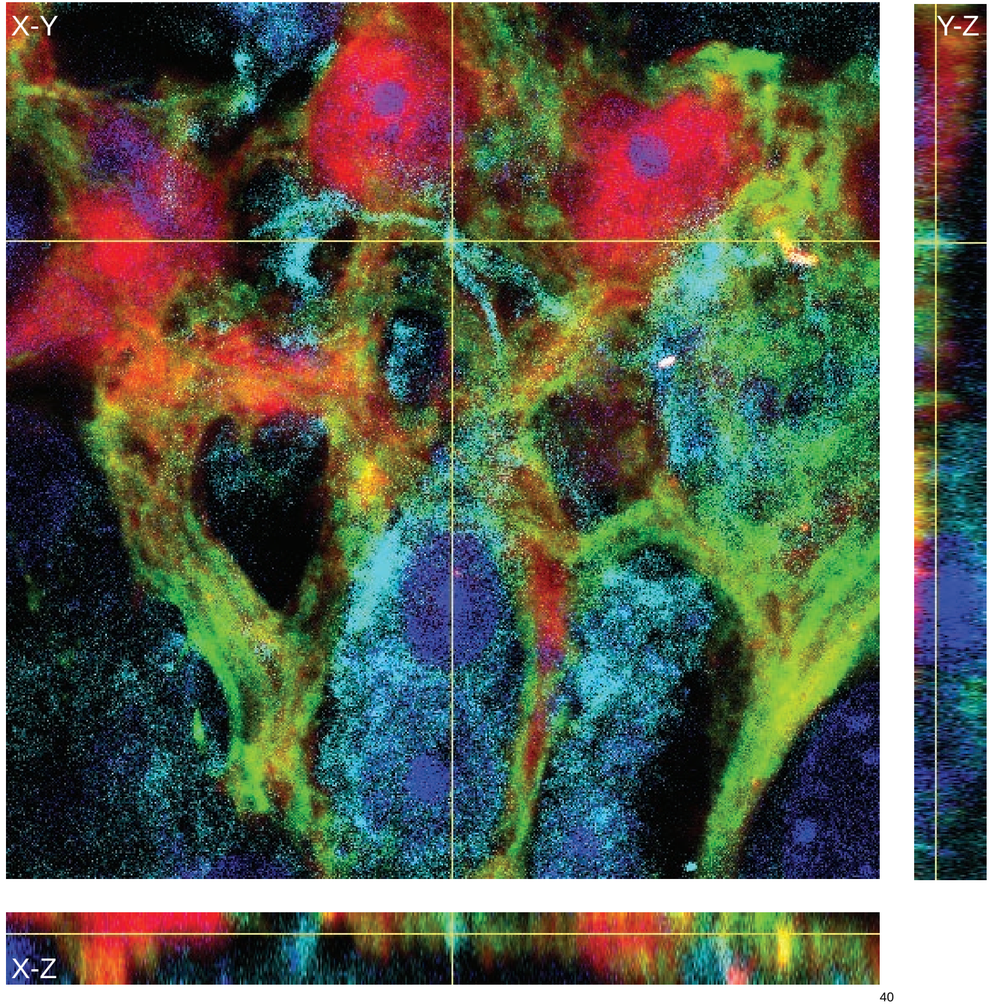

Figure 5

Fig 6: GDNF and HGF signaling regulate age-dependent changes in NENs and MENs proportions.

(A, B) Immunostaining myenteric plexus tissue from juvenile and mature Wnt1-cre:*Rosa26*-tdTomato mice with antibodies against the pan-neuronal marker HuC/D (green).

(C) Age-associated loss of NENs and gain of MENs in the small intestinal LM-MP of maturing and aging Wnt1-cre:*Rosa26*-tdTomato mice. Data represent mean ± S.E.M. ($p < 0.0001$).

(D) Western blot analyses of GDNF (green) and the house-keeping protein β-actin (red) expression in LM-MP tissues from mice of ages P10, P30, and P90. (n = 3 mice per group; each sample is a biological replicate). Fluorescent intensities of the two bands of GDNF (that correspond to ~25 kD bands of protein marker) were quantified together. The lower band of GDNF is present only in the P10 tissues and disappears in P30 and P90 adult murine tissues.

(E) Western blot analyses of HGF (green) and the house-keeping protein β-Actin (red) expression in LM-MP tissues from mice of ages P10, P30, and P90. (n = 3 mice per group; each sample is a biological replicate). Fluorescent intensities of the two bands of HGF (that are between 50 kD and 37 kD bands of the protein marker) were quantified together.

(F) The normalized fluorescent intensity of HGF protein to house-keeping protein β-Actin was compared between the three age groups. HGF expression significantly increased from P10 through P90. Data represent mean ± S.E.M. ($p = 0.02$).

(G) Age-dependent increase in Hgf mRNA transcript expression (normalized to the house-keeping gene Hprt) in the myenteric plexuses of P10, P30, and P90 old mice. Data represent mean ± S.E.M. ($p < 0.0001$).

(H) The normalized fluorescent intensity of GDNF protein to house-keeping protein β-Actin compared between the three age groups. GDNF presence was highest in P10 group and was significantly reduced in P30 and P90 groups. Data represent mean ± S.E.M. ($p = 0.0348$).

(I) Percent proportions of tdTomato^{-} MENs and mean HuC/D^{+} neurons/ganglia in LM-MP of cohorts of Wnt1-cre:*Rosa26*-tdTomato mice that were dosed with HGF or Saline from P10 to P20 age. Data represent mean ± S.E.M. (*** $p < 0.001$).

(J) Percent proportions of tdTomato^{-} MENs and mean HuC/D^{+} neurons/ganglia in LM-MP of cohorts of Wnt1-cre:*Rosa26*-tdTomato mice that were dosed with GDNF or Saline from P10 to P20 age. Data represent mean ± S.E.M. (*** $p < 0.001$).

(K) Percent proportions of tdTomato^{-} MENs and mean HuC/D^{+} neurons/ganglia in LM-MP of cohorts of Wnt1-cre:*Rosa26*-tdTomato mice that were dosed with GDNF or Saline from P60 to P70 age. Data represent mean ± S.E.M. (*** $p < 0.001$).

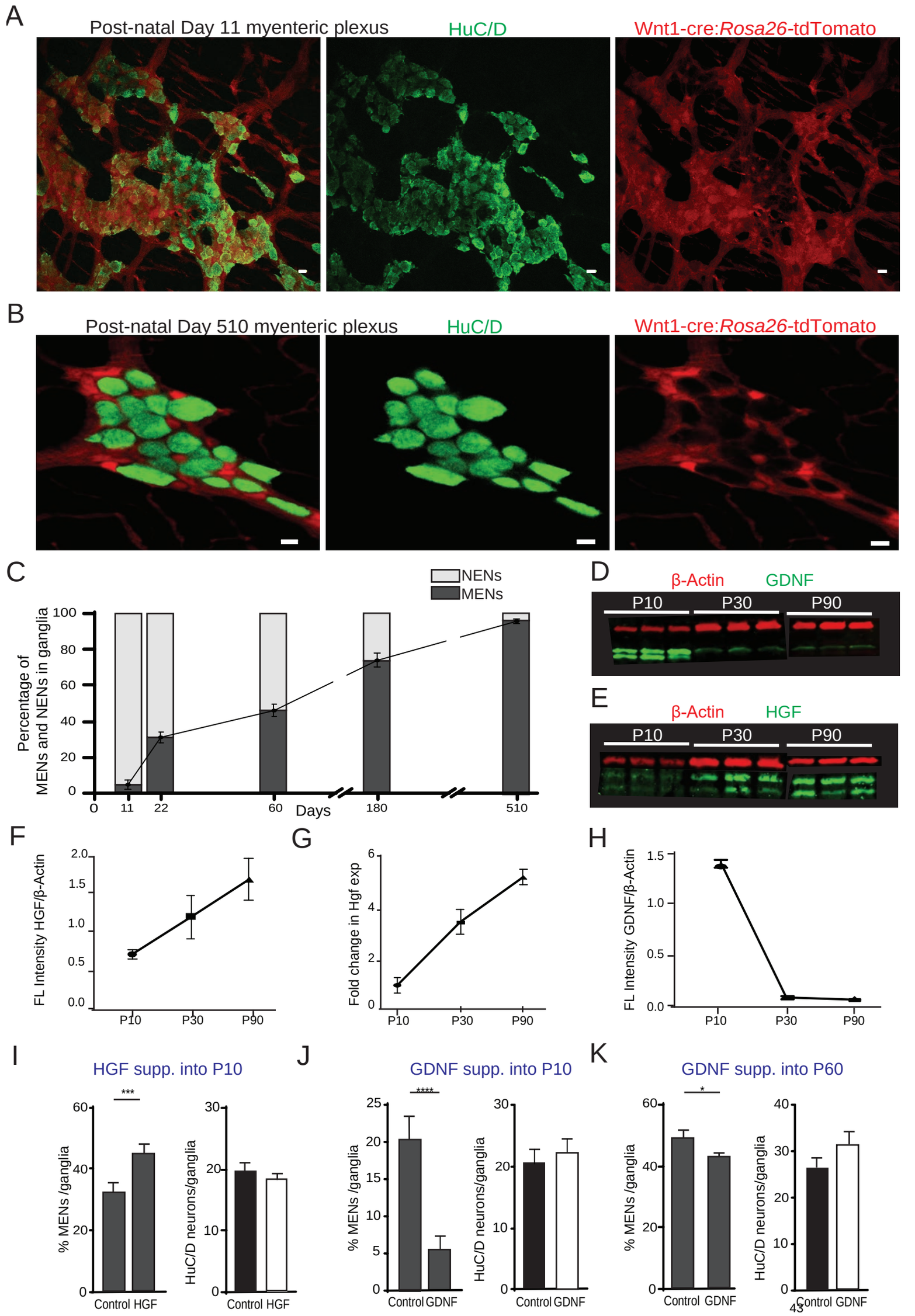
A
Post-natal Day 11 myenteric plexus
HuC/D
Wnt1-cre:Rosa26-tdTomato
B
Post-natal Day 510 myenteric plexus
HuC/D
Wnt1-cre:Rosa26-tdTomato
C
NENs
MENs
Percentage of MENs and NENs in ganglia
100
80
60
40
20
0
0
11
22
60
Days
180
510
D
β-Actin
GDNF
P10
P30
P90
E
β-Actin
HGF
P10
P30
P90
F
FL Intensity HGF/β-Actin
2.0
1.5
1.0
0.5
0.0
P10
P30
P90
G
Fold change in Hgf exp
6
4
2
0
P10
P30
P90
H
FL Intensity GDNF/β-Actin
1.5
1.0
0.5
0.0
P10
P30
P90
I
HGF supp. into P10
***
% MENs /ganglia
60
40
20
0
Control HGF
HuC/D neurons/ganglia
30
20
10
0
Control HGF
J
GDNF supp. into P10
****
% MENs /ganglia
25
20
15
10
5
0
Control GDNF
HuC/D neurons/ganglia
30
20
10
0
Control GDNF
K
GDNF supp. into P60
*
% MENs /ganglia
60
40
20
0
Control GDNF
HuC/D neurons/ganglia
40
30
20
10
0
Control GDNF

Figure 6

Fig 7: Reduced RET signaling accelerates ENS aging to cause pathology

(A) HuC/D immunostaining (green) LM-MP tissues from 16-week-old Ret $^{+/CFP}$ (Ret$^{+/-}$) mouse shows mutually exclusive expression of Ret-CFP (cyan, green arrow) and MHCst (red, red arrow) MENs. Nuclei are stained with DAPI (blue). Scale bar = 10 µm.

(B) Quantification of Ret-CFP^{+} neurons from 9- and 16-week-old Ret$^{+/-}$ mice show age-associated loss of Ret-CFP^{+} neurons. Data represent mean ± S.E.M. (* $p < 0.05$).

(C) Quantification of MHCst^{+} MENs shows significant increase in their proportions in Ret$^{+/-}$ mice but not in Ret$^{+/+}$ mice with age. Data represent mean ± S.E.M. (**** $p < 0.0001$).

(D) Measures of whole gut transit time (WGTT) in cohorts of Ret$^{+/-}$ and Ret$^{+/+}$ mice MENs show significant slowing of whole gut transit of Ret$^{+/-}$ but not Ret$^{+/+}$ mice with age. Data represent mean ± S.E.M. (* = $p < 0.05$).

A

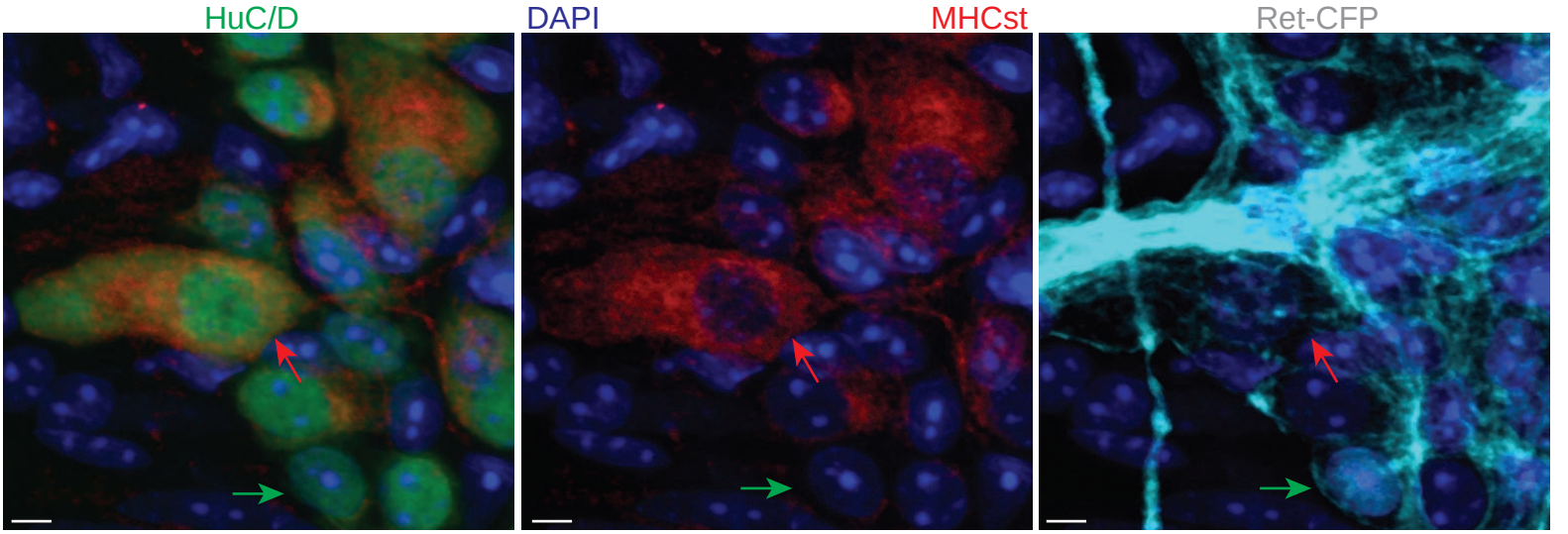

B

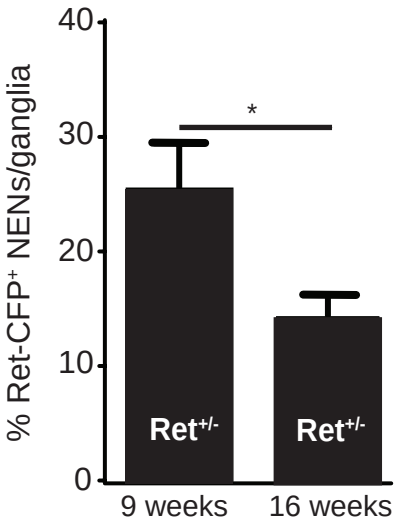

C

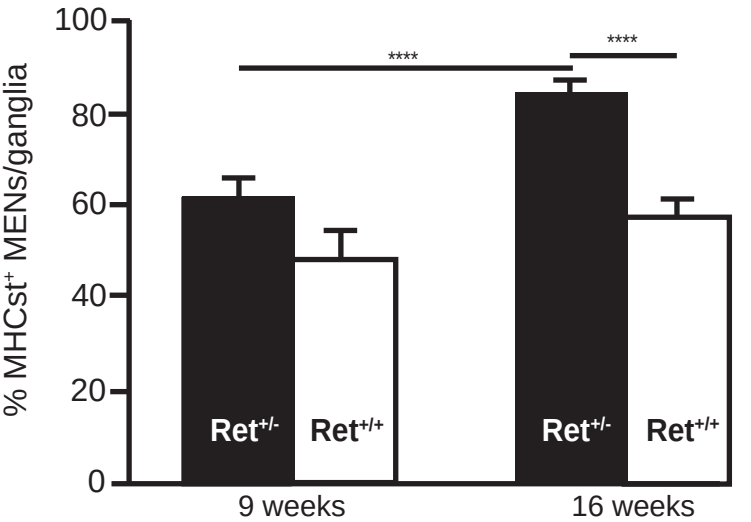

D

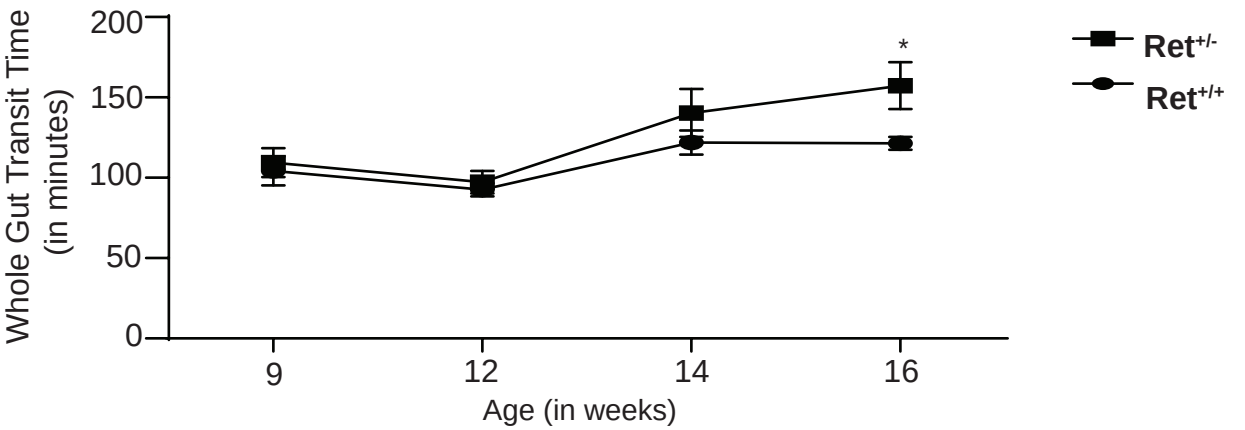

Figure 7

Fig 8: GDNF normalizes altered intestinal motility by increasing NENs proportions in the aging gut.

(A). Measures of whole gut transit time (WGTT) in GDNF (treated with GDNF) and Control (treated with Saline) cohorts of 17-month-old mice taken before the start of treatments and after the end of 10 consecutive days of treatment shows that the two groups are matched in their transit times before treatment, but GDNF treatment significant decreases average transit times when compared to the control cohort. Data represent mean ± S.E.M. (*** = $p < 0.001$).

(B). Quantification of percent MHCst^{+} MENs per HuC/D-labeled neurons in myenteric ganglia in the GDNF and Control cohorts shows significant decrease in their proportions in GDNF-treated cohort but not in saline-treated control cohort. Data represent mean ± S.E.M. (**** $p < 0.0001$).

(C). Quantification of numbers of RET^{+} NENs per myenteric ganglia shows significant increase in their numbers in GDNF cohort mice when compared with Control cohort mice. Data represent mean ± S.E.M. (**** $p < 0.0001$).

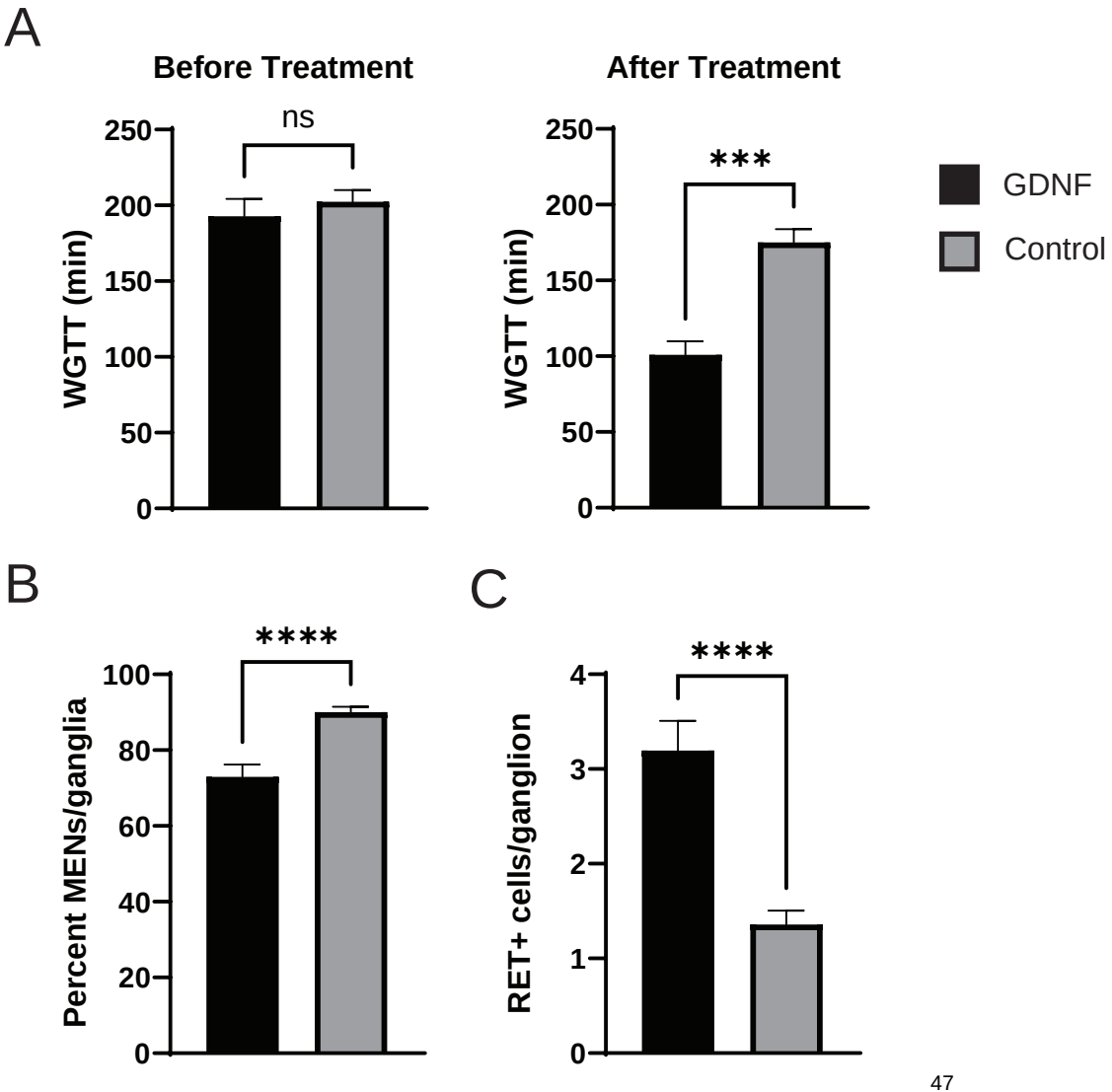
A
Before Treatment
After Treatment
ns
***
WGTT (min)
250
200
150
100
50
0
GDNF
Control
B
C
****
Percent MENs/ganglia
100
80
60
40
20
RET+ cells/ganglion
4
3
2
1

Figure 8

Fig 9: Presence of putative MENs and their molecular regulatory mechanisms in the human gut.

(A) Putative human MENs (red arrows) and NENs (green arrows) identified by presence or absence of the murine MENs markers, MET (blue) and MHCst (red) in subpopulations of HuC/D^{+} (green) small intestinal myenteric neurons from normal human duodenal tissue.

(B) Non-negative matrix factorization (NMF) was used to decompose our murine scRNAseq data from adult LM-MP tissues into 50 distinct latent spaces (called NMF patterns), of which four NMF patterns were found to be specific to MENs scRNAseq cell cluster.

(C) MENs-specific NMF patterns 32 and 41 were significantly upregulated in bulk-RNAseq of OD patients compared to controls. Data represent mean ± S.E.M.

A

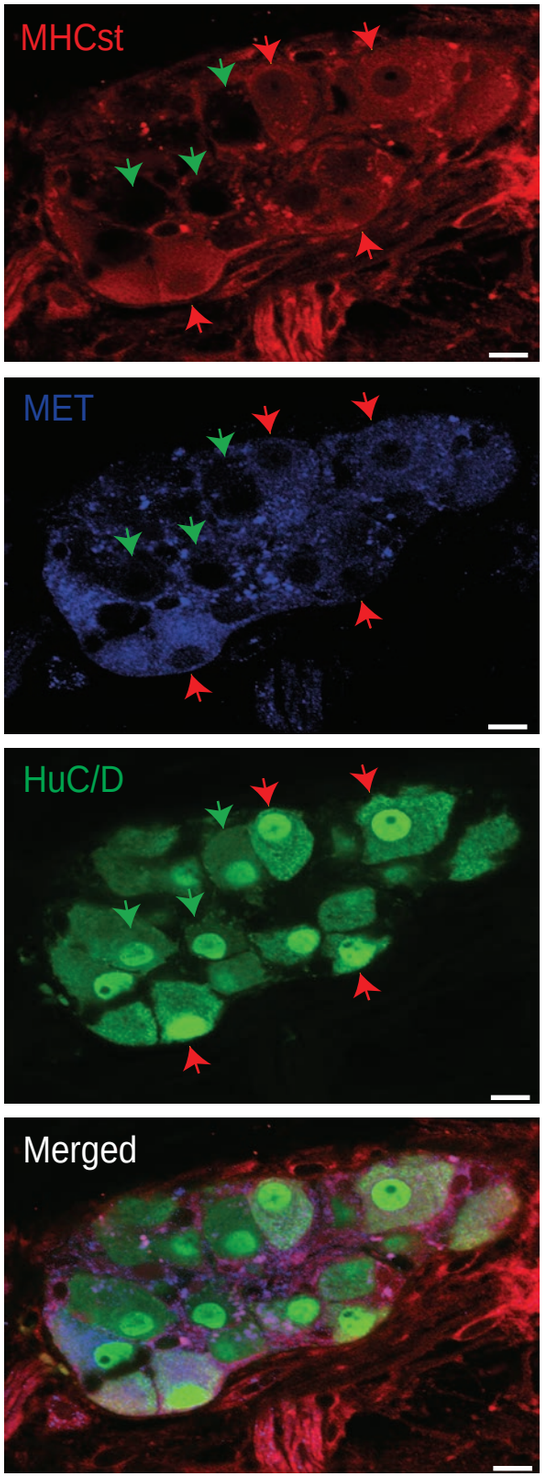
MHCst
MET
HuC/D
Merged

B

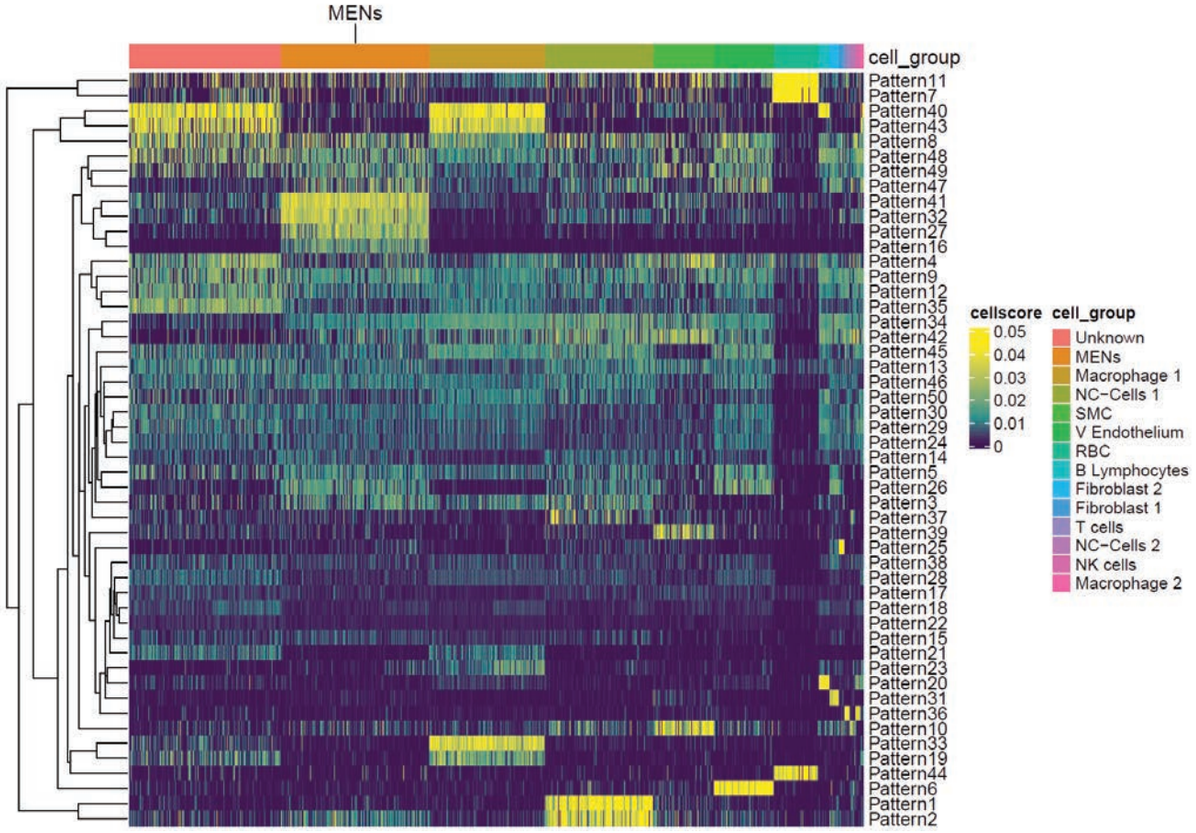
MENs
cell_group
Pattern11
Pattern7
Pattern40
Pattern43
Pattern8
Pattern48
Pattern49
Pattern47
Pattern41
Pattern32
Pattern27
Pattern16
Pattern4
Pattern9
Pattern12
Pattern35
Pattern34
Pattern42
Pattern45
Pattern13
Pattern46
Pattern50
Pattern30
Pattern29
Pattern24
Pattern14
Pattern5
Pattern26
Pattern3
Pattern37
Pattern39
Pattern25
Pattern38
Pattern28
Pattern17
Pattern18
Pattern22
Pattern15
Pattern21
Pattern23
Pattern20
Pattern31
Pattern36
Pattern10
Pattern33
Pattern19
Pattern44
Pattern6
Pattern1
Pattern2
cellscore
0.05
0.04
0.03
0.02
0.01
0
cell_group
Unknown
MENs
Macrophage 1
NC−Cells 1
SMC
V Endothelium
RBC
B Lymphocytes
Fibroblast 2
Fibroblast 1
T cells
NC−Cells 2
NK cells
Macrophage 2

C

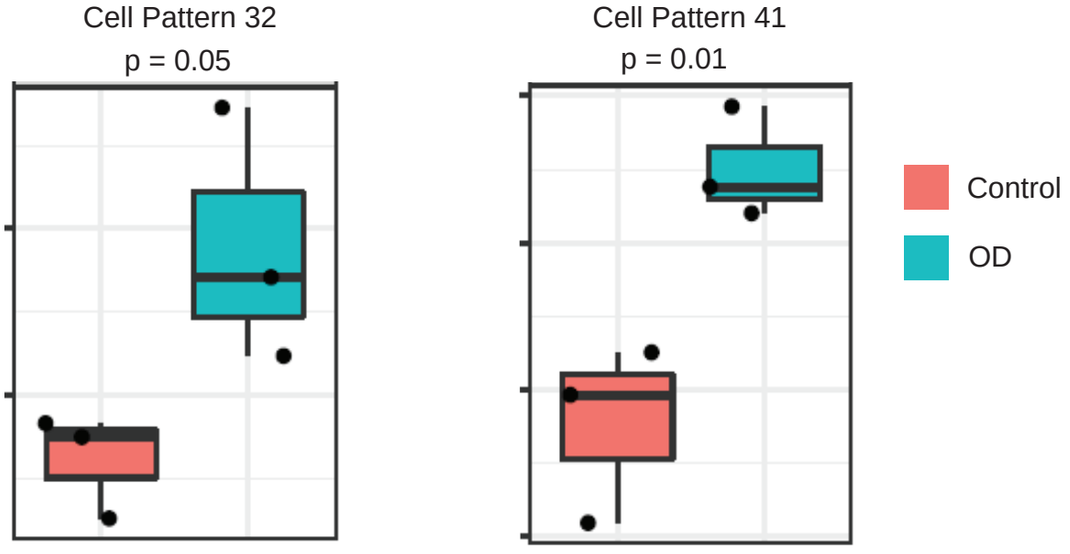
Cell Pattern 32
p = 0.05
Cell Pattern 41
p = 0.01
Control
OD

Figure 9

References

1 Kulkarni, S. *et al.* Advances in Enteric Neurobiology: The "Brain" in the Gut in Health and Disease. *J Neurosci* **38**, 9346-9354, doi:10.1523/JNEUROSCI.1663-18.2018 (2018).

2 Jarret, A. *et al.* Enteric Nervous System-Derived IL-18 Orchestrates Mucosal Barrier Immunity. *Cell* **180**, 50-63 e12, doi:10.1016/j.cell.2019.12.016 (2020).

3 Uesaka, T., Young, H. M., Pachnis, V. & Enomoto, H. Development of the intrinsic and extrinsic innervation of the gut. *Dev Biol* **417**, 158-167, doi:10.1016/j.ydbio.2016.04.016 (2016).

4 Obermayr, F., Hotta, R., Enomoto, H. & Young, H. M. Development and developmental disorders of the enteric nervous system. *Nat Rev Gastroenterol Hepatol* **10**, 43-57, doi:10.1038/nrgastro.2012.234 (2013).

5 Hao, M. M. & Young, H. M. Development of enteric neuron diversity. *J Cell Mol Med* **13**, 1193-1210, doi:10.1111/j.1582-4934.2009.00813.x (2009).

6 Anderson, R. B., Newgreen, D. F. & Young, H. M. Neural crest and the development of the enteric nervous system. *Adv Exp Med Biol* **589**, 181-196, doi:10.1007/978-0-387-46954-6_11 (2006).

7 Young, H. M. & Newgreen, D. Enteric neural crest-derived cells: origin, identification, migration, and differentiation. *Anat Rec* **262**, 1-15, doi:10.1002/1097-0185(20010101)262:1<1::AID-AR1006>3.0.CO;2-2 (2001).

8 Young, H. M., Hearn, C. J. & Newgreen, D. F. Embryology and development of the enteric nervous system. *Gut* **47 Suppl 4**, iv12-14; discussion iv26, doi:10.1136/gut.47.suppl_4.iv12 (2000).

9 Bergner, A. J. *et al.* Birthdating of myenteric neuron subtypes in the small intestine of the mouse. *J Comp Neurol* **522**, 514-527, doi:10.1002/cne.23423 (2014).

10 Uesaka, T., Nagashimada, M. & Enomoto, H. Neuronal Differentiation in Schwann Cell Lineage Underlies Postnatal Neurogenesis in the Enteric Nervous System. *J Neurosci* **35**, 9879-9888, doi:10.1523/JNEUROSCI.1239-15.2015 (2015).

11 Espinosa-Medina, I. *et al.* Dual origin of enteric neurons in vagal Schwann cell precursors and the sympathetic neural crest. *Proc Natl Acad Sci U S A* **114**, 11980-11985, doi:10.1073/pnas.1710308114 (2017).

12 Burns, A. J. Migration of neural crest-derived enteric nervous system precursor cells to and within the gastrointestinal tract. *Int J Dev Biol* **49**, 143-150, doi:10.1387/ijdb.041935ab (2005).

13 Laranjeira, C. *et al.* Glial cells in the mouse enteric nervous system can undergo neurogenesis in response to injury. *J Clin Invest* **121**, 3412-3424, doi:10.1172/JCI58200 (2011).

14 Brokhman, I. *et al.* Dual embryonic origin of the mammalian enteric nervous system. *Dev Biol* **445**, 256-270, doi:10.1016/j.ydbio.2018.11.014 (2019).

15 Sohal, G. S., Ali, M. M. & Farooqui, F. A. A second source of precursor cells for the developing enteric nervous system and interstitial cells of Cajal. *Int J Dev Neurosci* **20**, 619-626 (2002).

16 Habeck, M. VENT cells--a load of hot air? *Drug Discov Today* **8**, 332-333, doi:10.1016/s1359-6446(03)02663-1 (2003).

17 Saffrey, M. J. Cellular changes in the enteric nervous system during ageing. *Dev Biol* **382**, 344-355, doi:10.1016/j.ydbio.2013.03.015 (2013).

18 Becker, L., Kulkarni, S., Tiwari, G., Micci, M. A. & Pasricha, P. J. Divergent fate and origin of neurosphere-like bodies from different layers of the gut. *Am J Physiol Gastrointest Liver Physiol* **302**, G958-965, doi:10.1152/ajpgi.00511.2011 (2012).

19 Antal, M., Beneduce, B. M. & Regehr, W. G. The substantia nigra conveys target-dependent excitatory and inhibitory outputs from the basal ganglia to the thalamus. *J Neurosci* **34**, 8032-8042, doi:10.1523/JNEUROSCI.0236-14.2014 (2014).

20 Freyer, L., Aggarwal, V. & Morrow, B. E. Dual embryonic origin of the mammalian otic vesicle forming the inner ear. *Development* **138**, 5403-5414, doi:10.1242/dev.069849 (2011).

21 Honig, G., Liou, A., Berger, M., German, M. S. & Tecott, L. H. Precise pattern of recombination in serotonergic and hypothalamic neurons in a Pdx1-cre transgenic mouse line. *J Biomed Sci* **17**, 82, doi:10.1186/1423-0127-17-82 (2010).

22 Bardot, E. *et al.* Foxa2 identifies a cardiac progenitor population with ventricular differentiation potential. *Nat Commun* **8**, 14428, doi:10.1038/ncomms14428 (2017).

23 Burtscher, I., Barkey, W., Schwarzfischer, M., Theis, F. J. & Lickert, H. The Sox17-mCherry fusion mouse line allows visualization of endoderm and vascular endothelial development. *genesis* **50**, 496-505, doi:10.1002/dvg.20829 (2012).

24 Wilm, B., Ipenberg, A., Hastie, N. D., Burch, J. B. & Bader, D. M. The serosal mesothelium is a major source of smooth muscle cells of the gut vasculature. *Development* **132**, 5317-5328, doi:10.1242/dev.02141 (2005).

25 Kawaguchi, M., Bader, D. M. & Wilm, B. Serosal mesothelium retains vasculogenic potential. *Dev Dyn* **236**, 2973-2979, doi:10.1002/dvdy.21334 (2007).

26 Herrick, S. E. & Mutsaers, S. E. Mesothelial progenitor cells and their potential in tissue engineering. *Int J Biochem Cell Biol* **36**, 621-642, doi:10.1016/j.biocel.2003.11.002 (2004).

27 Chan, Sunny S.-K. *et al.* Mesp1 Patterns Mesoderm into Cardiac, Hematopoietic, or Skeletal Myogenic Progenitors in a Context-Dependent Manner. *Cell Stem Cell* **12**, 587-601, doi:10.1016/j.stem.2013.03.004 (2013).

28 Devine, W. P., Wythe, J. D., George, M., Koshiba-Takeuchi, K. & Bruneau, B. G. Early patterning and specification of cardiac progenitors in gastrulating mesoderm. *Elife* **3**, doi:10.7554/eLife.03848 (2014).

29 Lescroart, F. *et al.* Early lineage restriction in temporally distinct populations of Mesp1 progenitors during mammalian heart development. *Nat Cell Biol* **16**, 829-840, doi:10.1038/ncb3024 (2014).

30 Klotz, L. *et al.* Cardiac lymphatics are heterogeneous in origin and respond to injury. *Nature* **522**, 62-67, doi:10.1038/nature14483 (2015).

31 Chan, S. S. *et al.* Mesp1 patterns mesoderm into cardiac, hematopoietic, or skeletal myogenic progenitors in a context-dependent manner. *Cell Stem Cell* **12**, 587-601, doi:10.1016/j.stem.2013.03.004 (2013).

32 Baup, D., Moser, M., Schurmans, S. & Leo, O. Developmental regulation of the composite CAG promoter activity in the murine T lymphocyte cell lineage. *Genesis* **47**, 799-804, doi:10.1002/dvg.20569 (2009).

33 Alexopoulou, A. N., Couchman, J. R. & Whiteford, J. R. The CMV early enhancer/chicken beta actin (CAG) promoter can be used to drive transgene expression during the differentiation of murine embryonic stem cells into vascular progenitors. *BMC Cell Biol* **9**, 2, doi:10.1186/1471-2121-9-2 (2008).

34 Hu, X. *et al.* Reprogramming progressive cells display low CAG promoter activity. *Stem Cells* **39**, 43-54, doi:10.1002/stem.3295 (2021).

35 Akagi, Y. *et al.* Transcriptional activation of a hybrid promoter composed of cytomegalovirus enhancer and beta-actin/beta-globin gene in glomerular epithelial cells in vivo. *Kidney Int* **51**, 1265-1269, doi:10.1038/ki.1997.172 (1997).

36 Agah, R. *et al.* Gene recombination in postmitotic cells. Targeted expression of Cre recombinase provokes cardiac-restricted, site-specific rearrangement in adult ventricular muscle in vivo. *J Clin Invest* **100**, 169-179, doi:10.1172/JCI119509 (1997).

37 Sokoloff, A. J., Li, H. & Burkholder, T. J. Limited expression of slow tonic myosin heavy chain in human cranial muscles. *Muscle Nerve* **36**, 183-189, doi:10.1002/mus.20797 (2007).

38 Stockdale, F. E. & Miller, J. B. The cellular basis of myosin heavy chain isoform expression during development of avian skeletal muscles. *Dev Biol* **123**, 1-9, doi:10.1016/0012-1606(87)90420-9 (1987).

39 Miller, J. B., Crow, M. T. & Stockdale, F. E. Slow and fast myosin heavy chain content defines three types of myotubes in early muscle cell cultures. *J Cell Biol* **101**, 1643-1650, doi:10.1083/jcb.101.5.1643 (1985).

40 Vaughan, S. K., Stanley, O. L. & Valdez, G. Impact of Aging on Proprioceptive Sensory Neurons and Intrafusal Muscle Fibers in Mice. *J Gerontol A Biol Sci Med Sci* **72**, 771-779, doi:10.1093/gerona/glw175 (2017).

41 Avetisyan, M. *et al.* Hepatocyte Growth Factor and MET Support Mouse Enteric Nervous System Development, the Peristaltic Response, and Intestinal Epithelial Proliferation in Response to Injury. *J Neurosci* **35**, 11543-11558, doi:10.1523/JNEUROSCI.5267-14.2015 (2015).

42 Rappolee, D. A., Iyer, A. & Patel, Y. Hepatocyte growth factor and its receptor are expressed in cardiac myocytes during early cardiogenesis. *Circ Res* **78**, 1028-1036, doi:10.1161/01.res.78.6.1028 (1996).

43 Mao, Y., Wang, B. & Kunze, W. Characterization of myenteric sensory neurons in the mouse small intestine. *J Neurophysiol* **96**, 998-1010, doi:10.1152/jn.00204.2006 (2006).

44 Abraira, V. E. *et al.* The Cellular and Synaptic Architecture of the Mechanosensory Dorsal Horn. *Cell* **168**, 295-310 e219, doi:10.1016/j.cell.2016.12.010 (2017).

45 Zeisel, A. *et al.* Molecular Architecture of the Mouse Nervous System. *Cell* **174**, 999-1014 e1022, doi:10.1016/j.cell.2018.06.021 (2018).

46 Drokhlyansky, E. *et al.* The Human and Mouse Enteric Nervous System at Single-Cell Resolution. *Cell* **182**, 1606-1622, doi:10.1016/j.cell.2020.08.00310.1101/746743 (2020).

47 De Giorgio, R., Arakawa, J., Wetmore, C. J. & Sternini, C. Neurotrophin-3 and neurotrophin receptor immunoreactivity in peptidergic enteric neurons. *Peptides* **21**, 1421-1426, doi:10.1016/s0196-9781(00)00286-2 (2000).

48 Barrenschee, M. *et al.* SNAP-25 is abundantly expressed in enteric neuronal networks and upregulated by the neurotrophic factor GDNF. *Histochem Cell Biol* **143**, 611-623, doi:10.1007/s00418-015-1310-x (2015).

49 Gianino, S., Grider, J. R., Cresswell, J., Enomoto, H. & Heuckeroth, R. O. GDNF availability determines enteric neuron number by controlling precursor proliferation. *Development* **130**, 2187-2198, doi:10.1242/dev.00433 (2003).

50 Natarajan, D., Marcos-Gutierrez, C., Pachnis, V. & de Graaff, E. Requirement of signalling by receptor tyrosine kinase RET for the directed migration of enteric nervous system progenitor cells during mammalian embryogenesis. *Development* **129**, 5151-5160 (2002).

51 Taraviras, S. *et al.* Signalling by the RET receptor tyrosine kinase and its role in the development of the mammalian enteric nervous system. *Development* **126**, 2785-2797 (1999).

52 Rodrigues, D. M., Li, A. Y., Nair, D. G. & Blennerhassett, M. G. Glial cell line-derived neurotrophic factor is a key neurotrophin in the postnatal enteric nervous system. *Neurogastroenterol Motil* **23**, e44-56, doi:10.1111/j.1365-2982.2010.01626.x (2011).

53 Amano, O. *et al.* Hepatocyte growth factor is essential for migration of myogenic cells and promotes their proliferation during the early periods of tongue morphogenesis in mouse embryos. *Dev Dyn* **223**, 169-179, doi:10.1002/dvdy.1228 (2002).

54 Wang, H. *et al.* The timing and location of glial cell line-derived neurotrophic factor expression determine enteric nervous system structure and function. *J Neurosci* **30**, 1523-1538, doi:10.1523/JNEUROSCI.3861-09.2010 (2010).

55 (!!! INVALID CITATION !!!).

56 Uesaka, T., Nagashimada, M., Yonemura, S. & Enomoto, H. Diminished Ret expression compromises neuronal survival in the colon and causes intestinal aganglionosis in mice. *J Clin Invest* **118**, 1890-1898, doi:10.1172/JCI34425 (2008).

57 Kim, M. *et al.* Obstructed defecation-an enteric neuropathy? An exploratory study of patient samples. *Int J Colorectal Dis* **34**, 193-196, doi:10.1007/s00384-018-3160-1 (2019).

58 Sun, T. *et al.* Aging-dependent decrease in the numbers of enteric neurons, interstitial cells of Cajal and expression of connexin43 in various regions of gastrointestinal tract. *Aging (Albany NY)* **10**, 3851-3865, doi:10.18632/aging.101677 (2018).

59 Becker, L. *et al.* Age-dependent shift in macrophage polarisation causes inflammation-mediated degeneration of enteric nervous system. *Gut* **67**, 827-836, doi:10.1136/gutjnl-2016-312940 (2018).

60 Sathyan, S. *et al.* Plasma proteomic profile of age, health span, and all-cause mortality in older adults. *Aging Cell* **n/a**, e13250, doi:10.1111/acel.13250.

61 Stein-O'Brien, G. L. *et al.* Decomposing Cell Identity for Transfer Learning across Cellular Measurements, Platforms, Tissues, and Species. *Cell Syst* **8**, 395-411 e398, doi:10.1016/j.cels.2019.04.004 (2019).

62 Stein-O'Brien, G. L. *et al.* Enter the Matrix: Factorization Uncovers Knowledge from Omics. *Trends Genet* **34**, 790-805, doi:10.1016/j.tig.2018.07.003 (2018).

63 Sharma, G., Colantuoni, C., Goff, L. A., Fertig, E. J. & Stein-O'Brien, G. projectR: an R/Bioconductor package for transfer learning via PCA, NMF, correlation and clustering. *Bioinformatics* **36**, 3592-3593, doi:10.1093/bioinformatics/btaa183 (2020).

64 Young, H. M. & Newgreen, D. Enteric neural crest-derived cells: Origin, identification, migration, and differentiation. *The Anatomical Record* **262**, 1-15, doi:10.1002/1097-0185(20010101)262:1<1::AID-AR1006>3.0.CO;2-2 (2001).

65 Prummel, K. D., Nieuwenhuize, S. & Mosimann, C. The lateral plate mesoderm. *Development* **147**, dev175059, doi:10.1242/dev.175059 (2020).

66 Xue, R. *et al.* Expression of Cystic Fibrosis Transmembrane Conductance Regulator in Ganglia of Human Gastrointestinal Tract. *Sci Rep* **6**, 30926, doi:10.1038/srep30926 (2016).

67 Morarach, K. *et al.* Diversification of molecularly defined myenteric neuron classes revealed by single cell RNA-sequencing. *bioRxiv*, 2020.2003.2002.955757, doi:10.1101/2020.03.02.955757 (2020).

68 May-Zhang, A. A. *et al.* Combinatorial Transcriptional Profiling of Mouse and Human Enteric Neurons Identifies Shared and Disparate Subtypes In Situ. *Gastroenterology*, doi:10.1053/j.gastro.2020.09.032 (2020).

69 Papaconstantinou, J. *et al.* Attenuation of p38alpha MAPK stress response signaling delays the in vivo aging of skeletal muscle myofibers and progenitor cells. *Aging (Albany NY)* **7**, 718-733, doi:10.18632/aging.100802 (2015).

70 Soret, R. *et al.* Glial Cell-Derived Neurotrophic Factor Induces Enteric Neurogenesis and Improves Colon Structure and Function in Mouse Models of Hirschsprung Disease. *Gastroenterology* **159**, 1824-1838 e1817, doi:10.1053/j.gastro.2020.07.018 (2020).

71 Kulkarni, S. *et al.* Adult enteric nervous system in health is maintained by a dynamic balance between neuronal apoptosis and neurogenesis. *Proc Natl Acad Sci U S A* **114**, E3709-E3718, doi:10.1073/pnas.1619406114 (2017).

72 Saffrey, M. J. Aging of the mammalian gastrointestinal tract: a complex organ system. *Age (Dordr)* **36**, 9603, doi:10.1007/s11357-013-9603-2 (2014).

73 Barrenschee, M. *et al.* No neuronal loss, but alterations of the GDNF system in asymptomatic diverticulosis. *PLoS One* **12**, e0171416, doi:10.1371/journal.pone.0171416 (2017).

74 Cossais, F. *et al.* Altered enteric expression of the homeobox transcription factor Phox2b in patients with diverticular disease. *United European Gastroenterology Journal* **7**, 349-357, doi:10.1177/2050640618824913 (2019).

75 Schafmayer, C. *et al.* Genome-wide association analysis of diverticular disease points towards neuromuscular, connective tissue and epithelial pathomechanisms. *Gut* **68**, 854, doi:10.1136/gutjnl-2018-317619 (2019).

76 Muller, P. A. *et al.* Microbiota-modulated CART(+) enteric neurons autonomously regulate blood glucose. *Science* **370**, 314-321, doi:10.1126/science.abd6176 (2020).

77 Matheis, F. *et al.* Adrenergic Signaling in Muscularis Macrophages Limits Infection-Induced Neuronal Loss. *Cell* **180**, 64-78 e16, doi:10.1016/j.cell.2019.12.002 (2020).

78 Becker, L., Kulkarni, S., Tiwari, G., Micci, M.-A. & Pasricha, P. J. Divergent fate and origin of neurosphere-like bodies from different layers of the gut. *American Journal of Physiology-Gastrointestinal and Liver Physiology* **302**, G958-G965, doi:10.1152/ajpgi.00511.2011 (2012).

79 Becker, L., Peterson, J., Kulkarni, S. & Pasricha, P. J. Ex vivo neurogenesis within enteric ganglia occurs in a PTEN dependent manner. *PLoS One* **8**, e59452 (2013).

80 Shenje, L. T. *et al.* Precardiac deletion of Numb and Numblike reveals renewal of cardiac progenitors. *Elife* **3**, e02164, doi:10.7554/eLife.02164 (2014).

81 Susaki, E. A. *et al.* Whole-brain imaging with single-cell resolution using chemical cocktails and computational analysis. *Cell* **157**, 726-739, doi:10.1016/j.cell.2014.03.042 (2014).

82 Bray, N. L., Pimentel, H., Melsted, P. & Pachter, L. Near-optimal probabilistic RNA-seq quantification. *Nat Biotechnol* **34**, 525-527, doi:10.1038/nbt.3519 (2016).

83 Haghverdi, L., Lun, A. T. L., Morgan, M. D. & Marioni, J. C. Batch effects in single-cell RNA-sequencing data are corrected by matching mutual nearest neighbors. *Nat Biotechnol* **36**, 421-427, doi:10.1038/nbt.4091 (2018).

84 Padovan-Merhar, O. *et al.* Single mammalian cells compensate for differences in cellular volume and DNA copy number through independent global transcriptional mechanisms. *Mol Cell* **58**, 339-352, doi:10.1016/j.molcel.2015.03.005 (2015).

85 Gu, Z., Eils, R. & Schlesner, M. Complex heatmaps reveal patterns and correlations in multidimensional genomic data. *Bioinformatics* **32**, 2847-2849, doi:10.1093/bioinformatics/btw313 (2016).

86 Tabula Muris, C. A single-cell transcriptomic atlas characterizes ageing tissues in the mouse. *Nature* **583**, 590-595, doi:10.1038/s41586-020-2496-1 (2020).

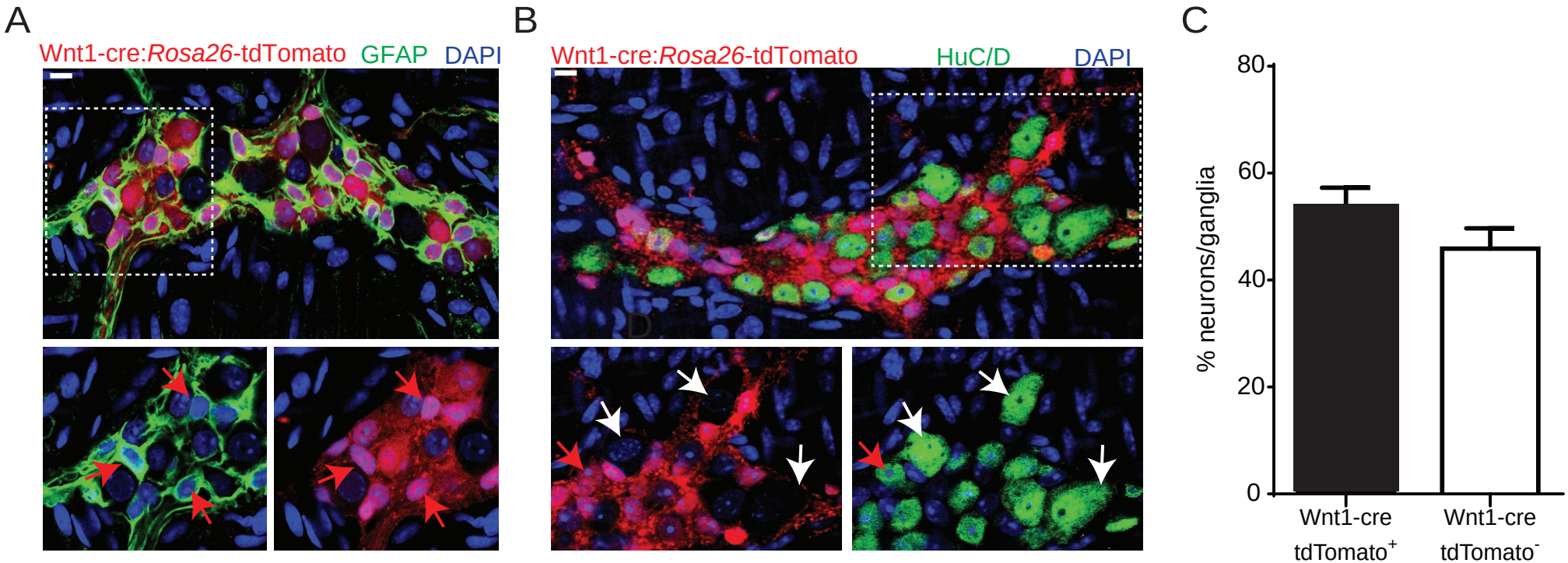
A
Wnt1-cre:Rosa26-tdTomato
GFAP
DAPI
B
Wnt1-cre:Rosa26-tdTomato
HuC/D
DAPI
C
% neurons/ganglia
80
60
40
20
0
Wnt1-cre tdTomato+
Wnt1-cre tdTomato-

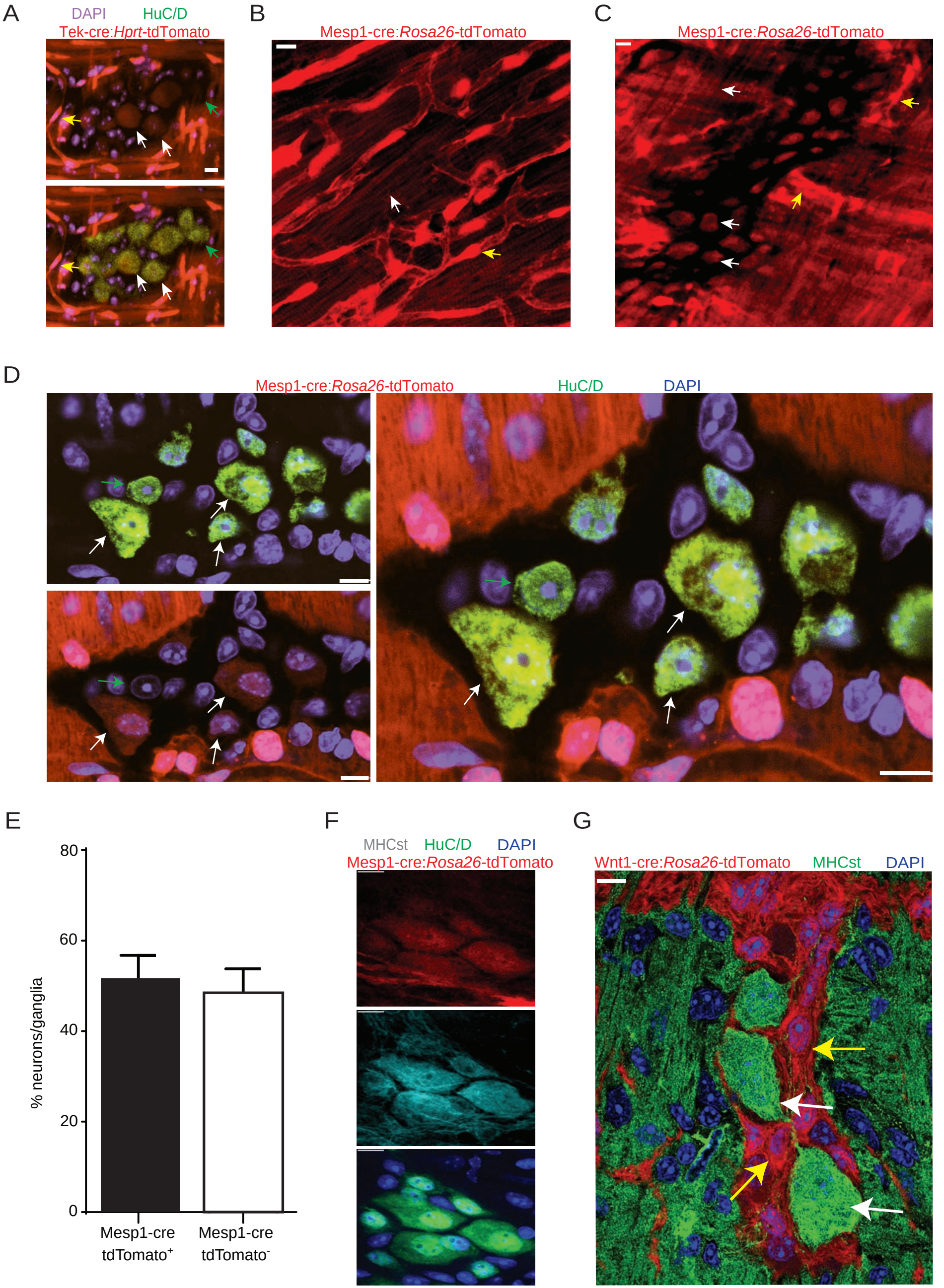
A
DAPI
HuC/D
Tek-cre:Hprt-tdTomato
B
Mesp1-cre:Rosa26-tdTomato
C
Mesp1-cre:Rosa26-tdTomato
D
Mesp1-cre:Rosa26-tdTomato
HuC/D
DAPI
E
% neurons/ganglia
80
60
40
20
0
Mesp1-cre tdTomato+
Mesp1-cre tdTomato-
F
MHCst
HuC/D
DAPI
Mesp1-cre:Rosa26-tdTomato
G
Wnt1-cre:Rosa26-tdTomato
MHCst
DAPI

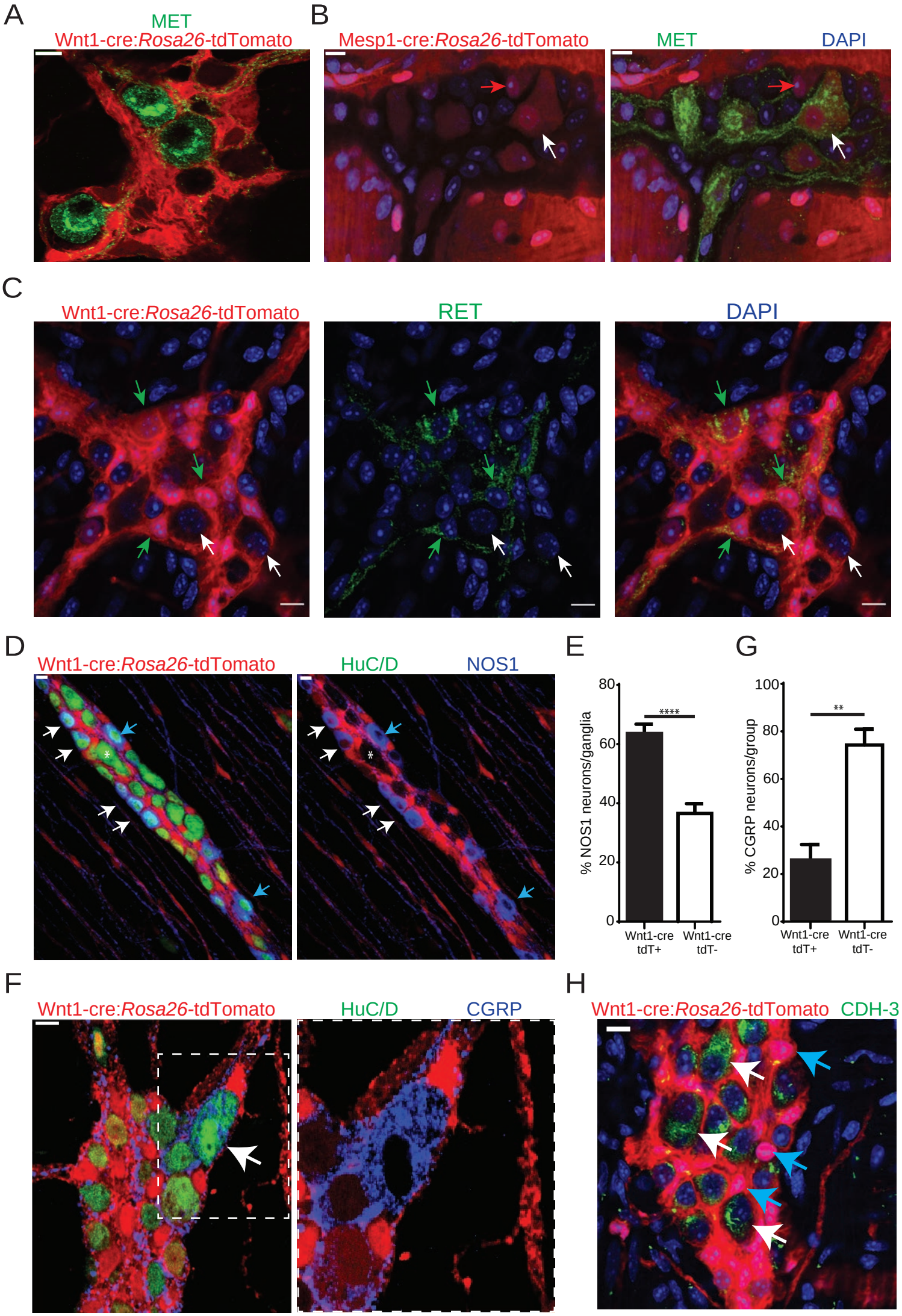
A
MET
Wnt1-cre:Rosa26-tdTomato
B
Mesp1-cre:Rosa26-tdTomato
MET
DAPI
C
Wnt1-cre:Rosa26-tdTomato
RET
DAPI
D
Wnt1-cre:Rosa26-tdTomato
HuC/D
NOS1
E
% NOS1 neurons/ganglia
80
60
40
20
0
****
Wnt1-cre tdT+
Wnt1-cre tdT-
G
% CGRP neurons/group
100
80
60
40
20
0
**
Wnt1-cre tdT+
Wnt1-cre tdT-
F
Wnt1-cre:Rosa26-tdTomato
HuC/D
CGRP
H
Wnt1-cre:Rosa26-tdTomato
CDH-3

A

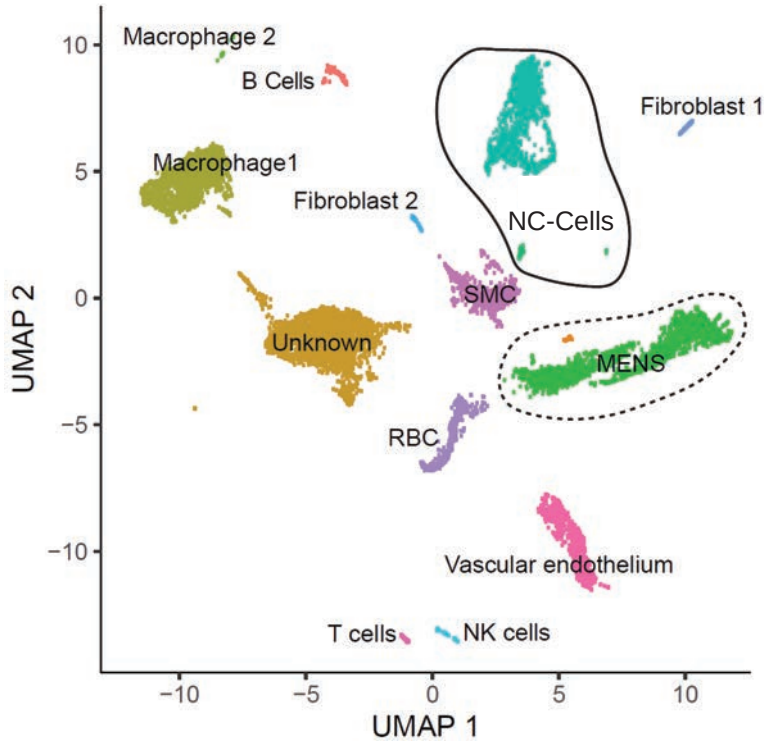
Macrophage 2
B Cells
Macrophage1
Fibroblast 2
Fibroblast 1
NC-Cells
SMC
Unknown
MENS
RBC
Vascular endothelium
T cells
NK cells
UMAP 2
UMAP 1
10
5
0
−5
−10
−10
−5
0
5
10

B

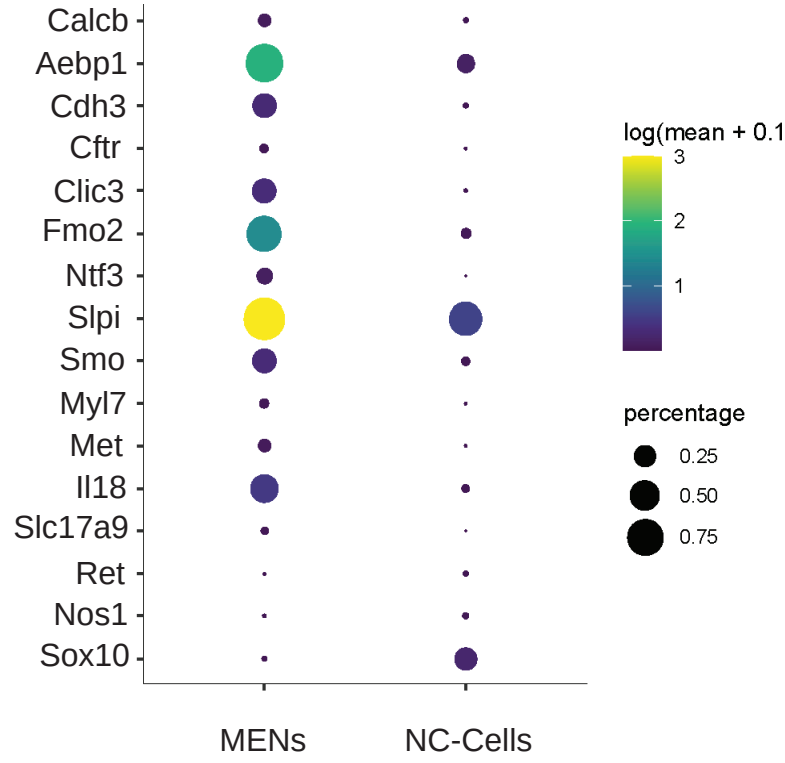
Calcb
Aebp1
Cdh3
Cftr
Clic3
Fmo2
Ntf3
Slpi
Smo
Myl7
Met
Il18
Slc17a9
Ret
Nos1
Sox10
MENs
NC-Cells
log(mean + 0.1)
3
2
1
percentage
0.25
0.50
0.75

C

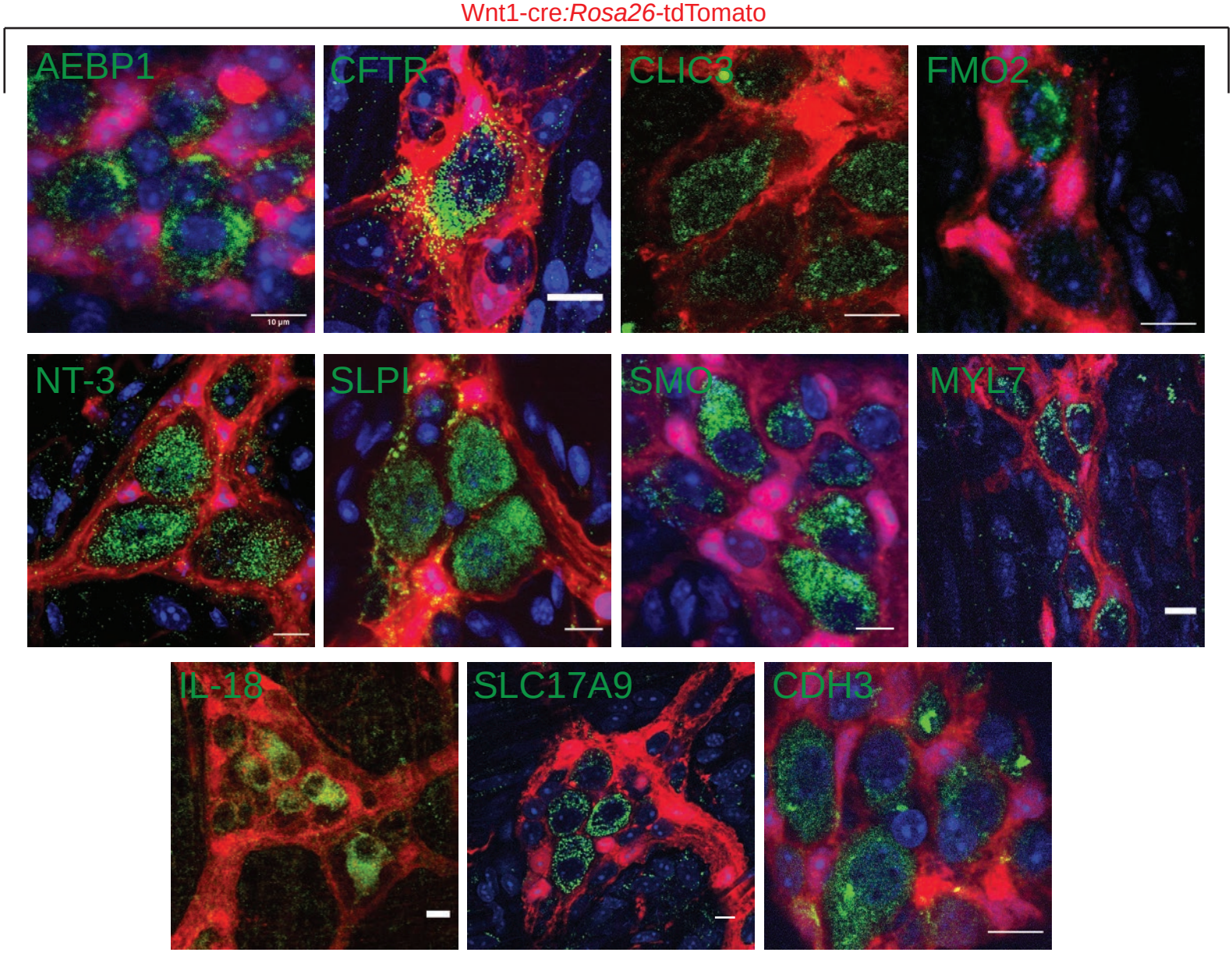
Wnt1-cre:Rosa26-tdTomato
AEBP1
CFTR
CLIC3
FMO2
NT-3
SLPI
SMC
MYL7
IL-18
SLC17A9
CDH3

A

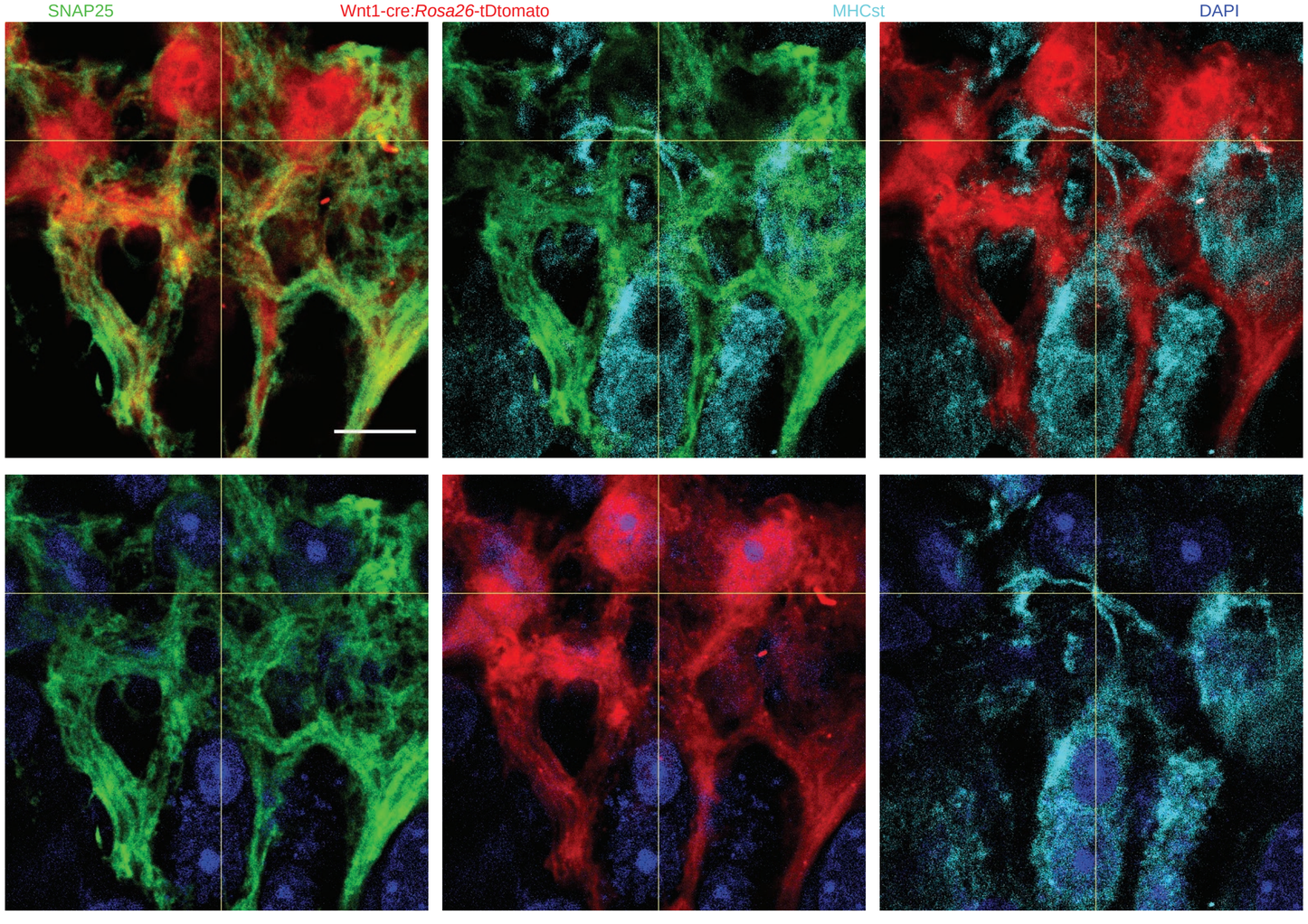

B

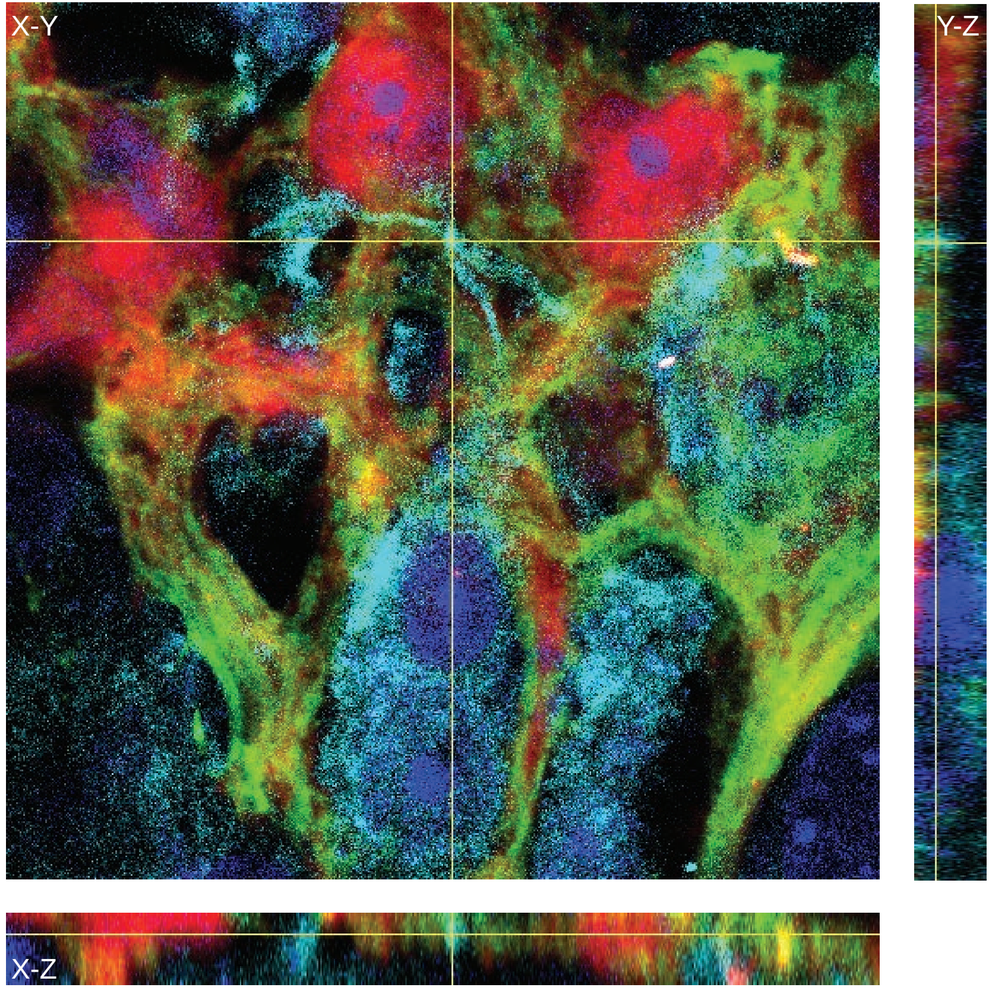

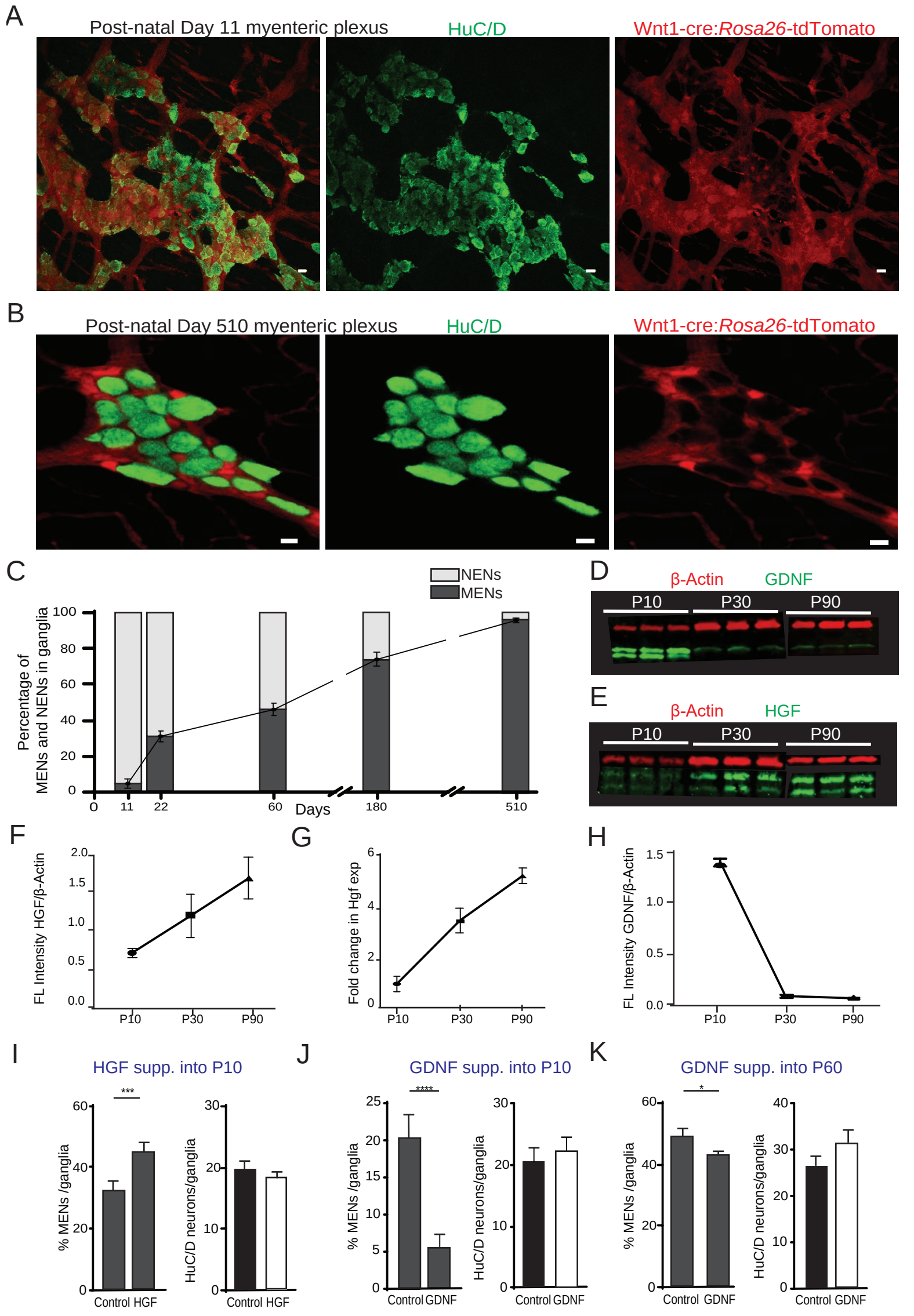
A
Post-natal Day 11 myenteric plexus
HuC/D
Wnt1-cre:Rosa26-tdTomato
B
Post-natal Day 510 myenteric plexus
HuC/D
Wnt1-cre:Rosa26-tdTomato
C
NENs
MENs
Percentage of MENs and NENs in ganglia
100
80
60
40
20
0
0
11
22
60
180
510
Days
D
β-Actin
GDNF
P10
P30
P90
E
β-Actin
HGF
P10
P30
P90
F
FL Intensity HGF/β-Actin
2.0
1.5
1.0
0.5
0.0
P10
P30
P90
G
Fold change in Hgf exp
6
4
2
0
P10
P30
P90
H
FL Intensity GDNF/β-Actin
1.5
1.0
0.5
0.0
P10
P30
P90
I
HGF supp. into P10
***
% MENs /ganglia
60
40
20
0
Control HGF
HuC/D neurons/ganglia
30
20
10
0
Control HGF
J
GDNF supp. into P10
****
% MENs /ganglia
25
20
15
10
5
0
Control GDNF
HuC/D neurons/ganglia
30
20
10
0
Control GDNF
K
GDNF supp. into P60
*
% MENs /ganglia
60
40
20
0
Control GDNF
HuC/D neurons/ganglia
40
30
20
10
0
Control GDNF

A

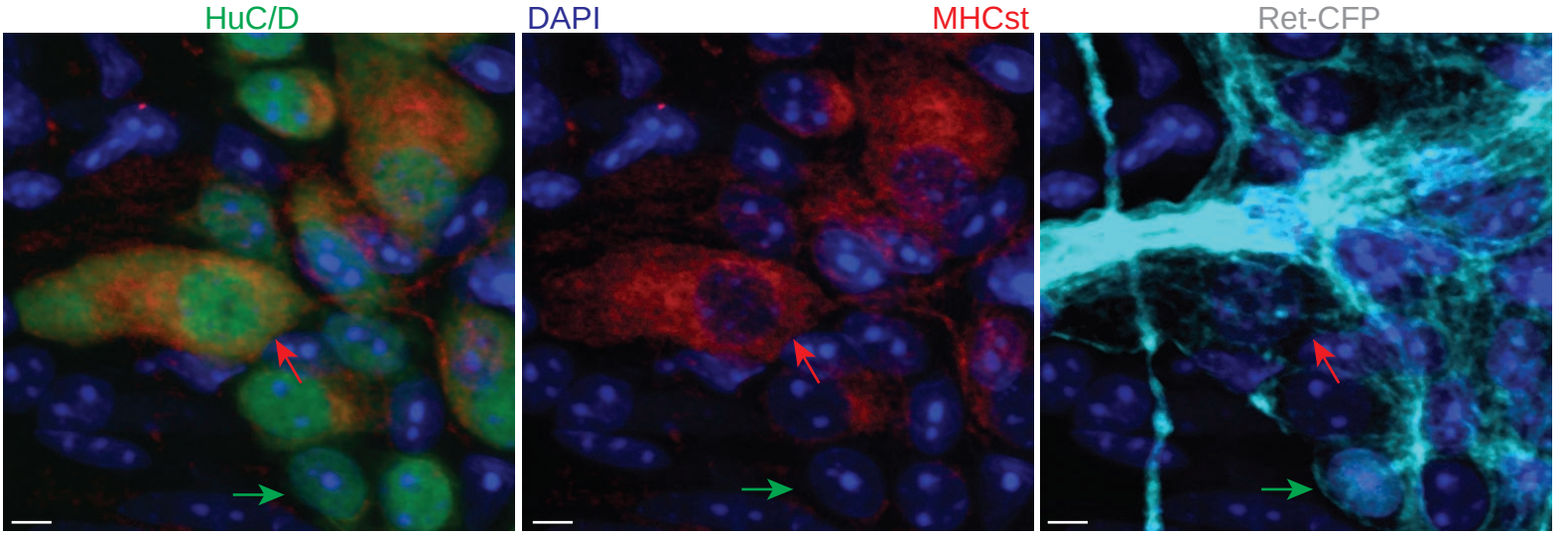
HuC/D
DAPI
MHCst
Ret-CFP

B

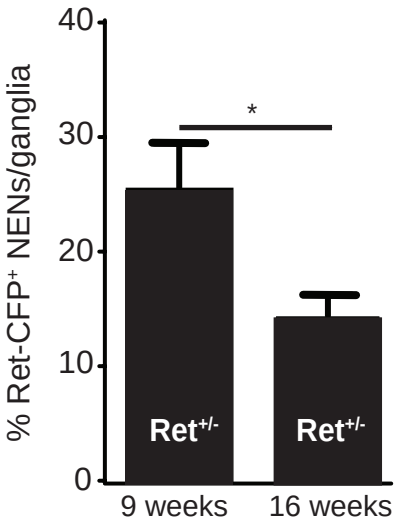
% Ret-CFP+ NENs/ganglia
40
30
20
10
0
*
Ret+/-
Ret+/-
9 weeks
16 weeks

C

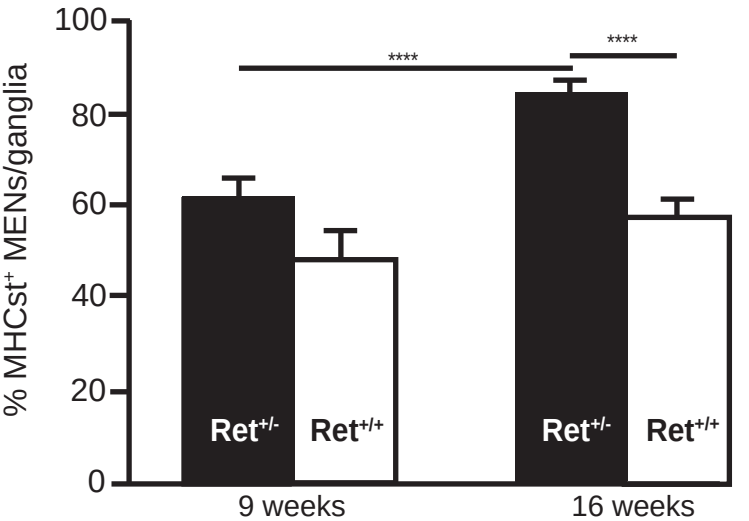
% MHCst+ MENs/ganglia
100
80
60
40
20
0
****
****
Ret+/-
Ret+/+
Ret+/-
Ret+/+
9 weeks
16 weeks

D

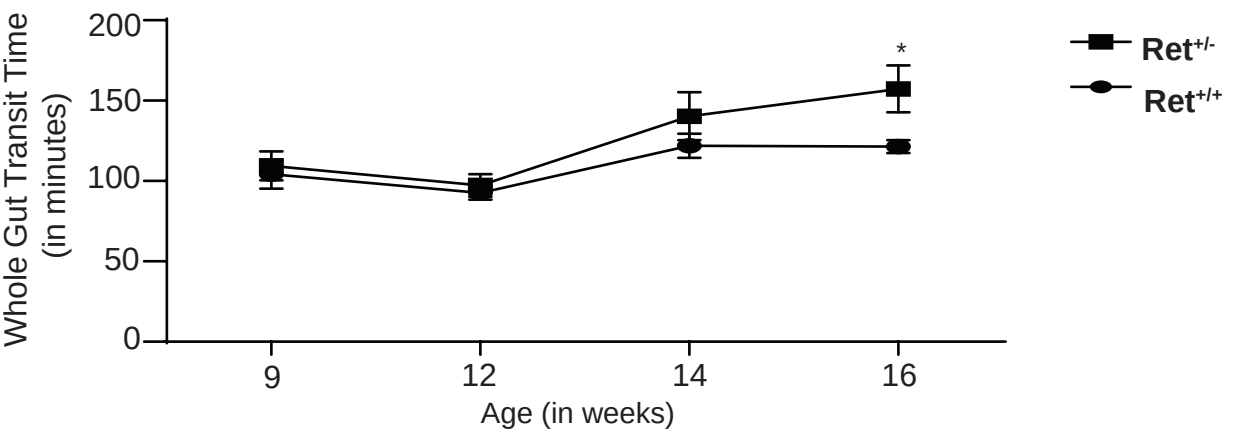
Whole Gut Transit Time (in minutes)
200
150
100
50
0
*
9
12
14
16
Age (in weeks)
Ret+/-
Ret+/+

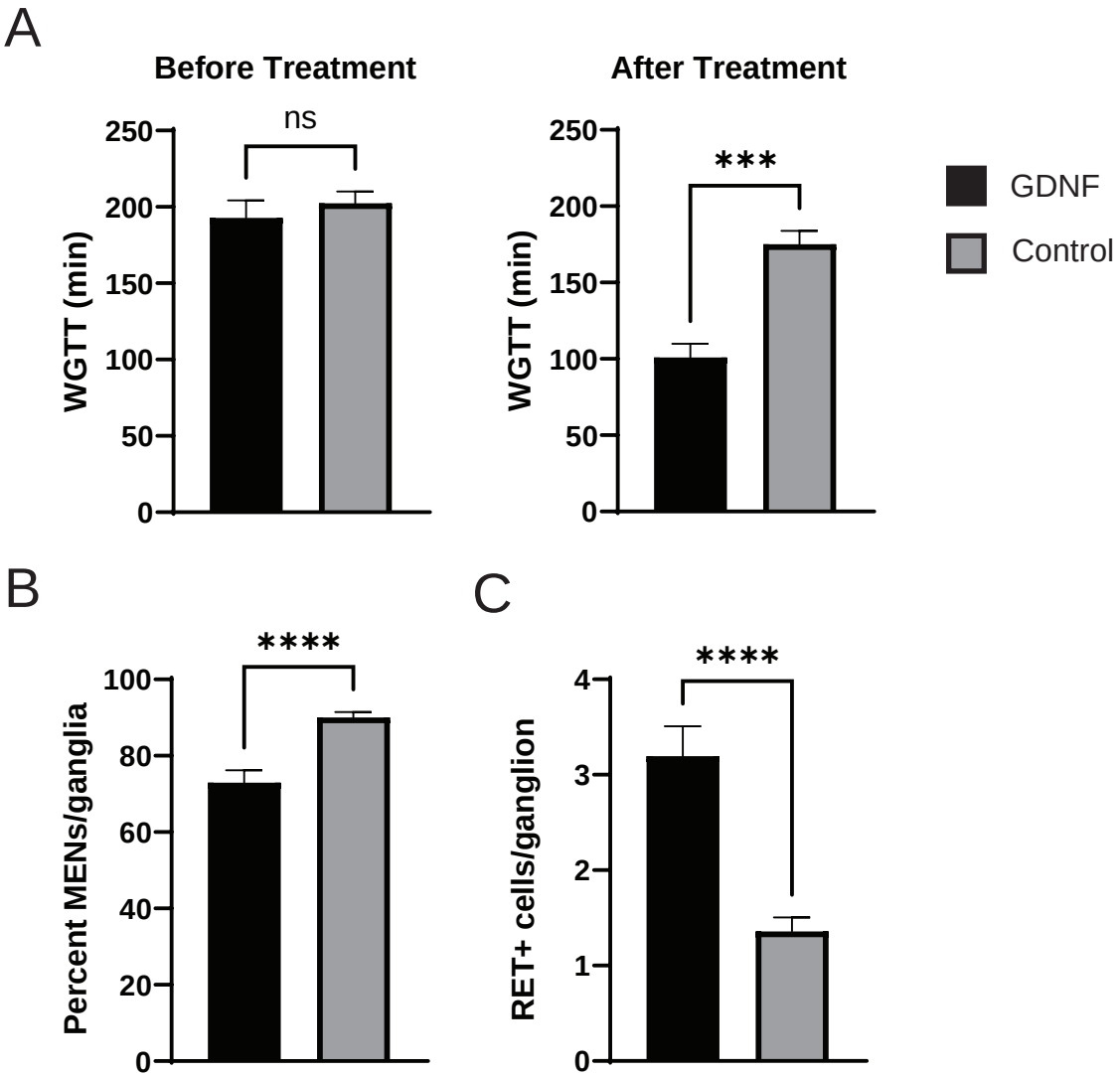
A
Before Treatment
After Treatment
ns
***
WGTT (min)
250
200
150
100
50
0
GDNF
Control
B
****
Percent MENs/ganglia
100
80
60
40
20
0
C
****
RET+ cells/ganglion
4
3
2
1
0

A

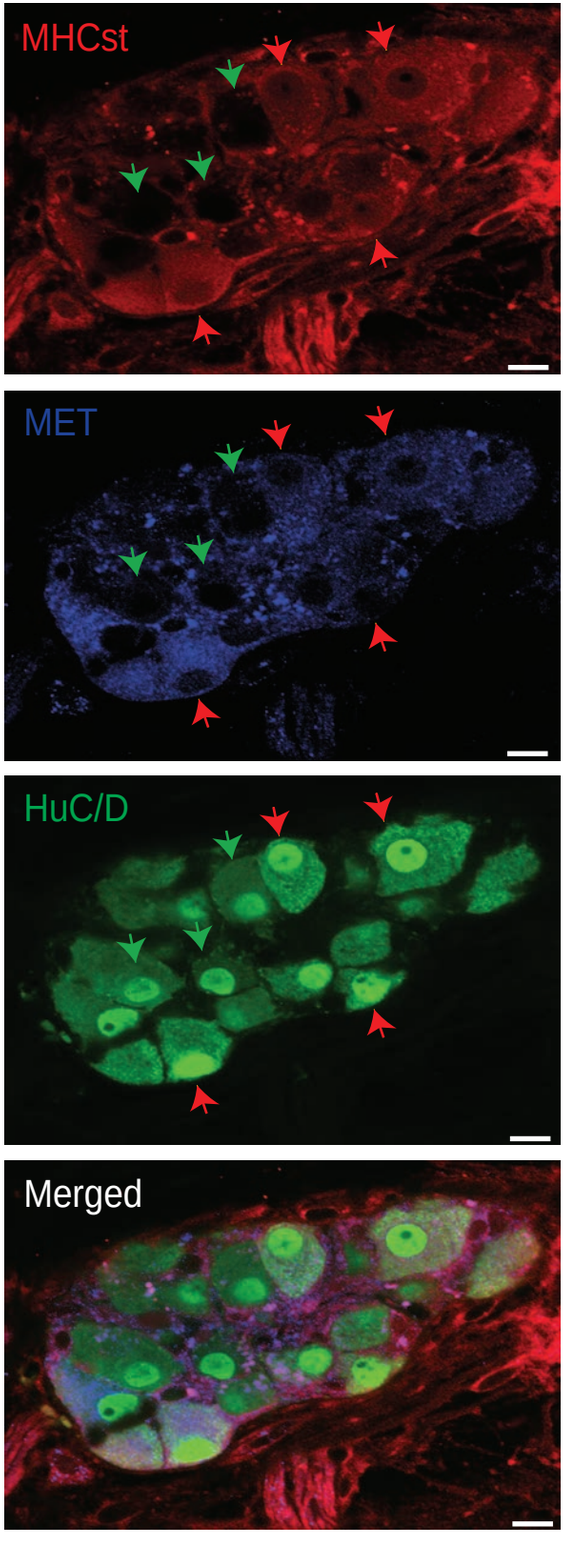
MHCst
MET
HuC/D
Merged

B

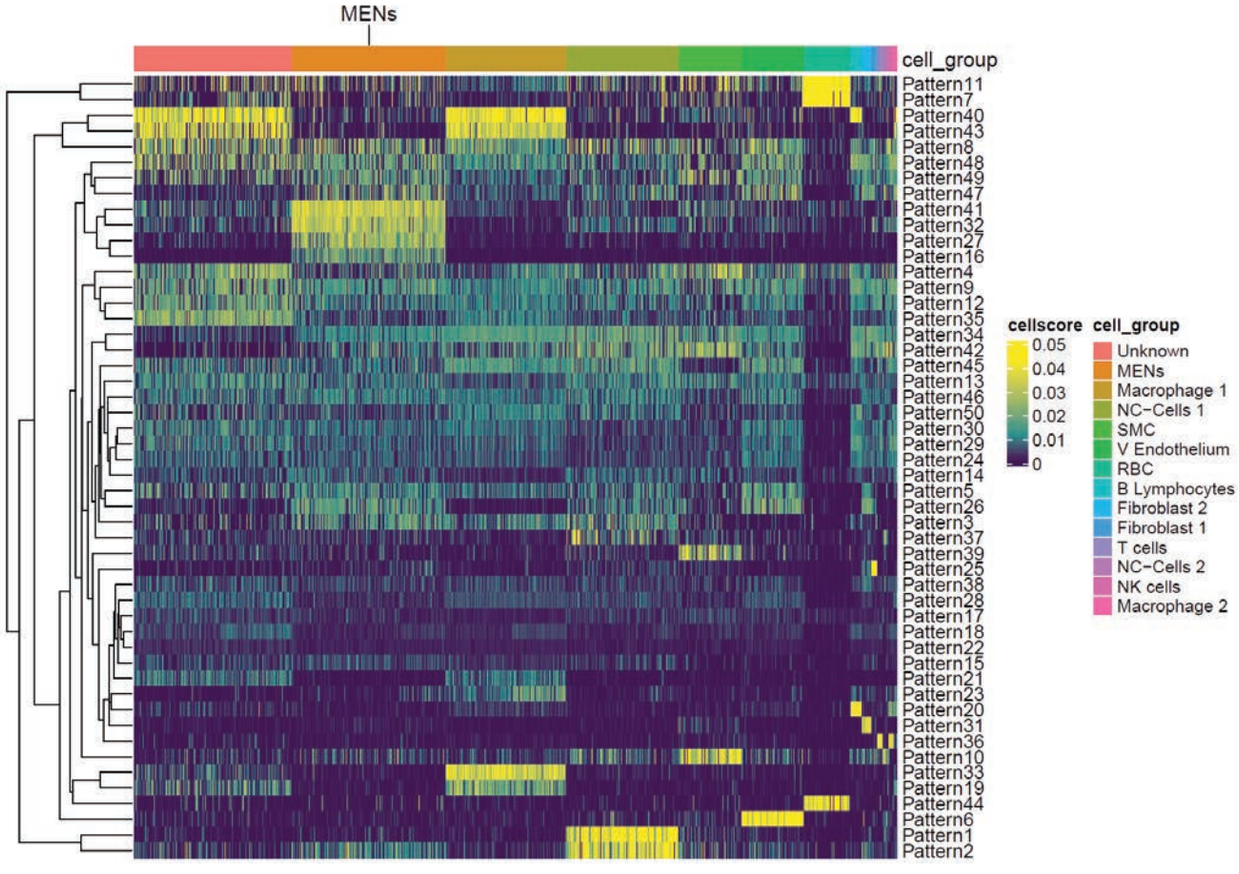
MENs
cell_group
Pattern11
Pattern7
Pattern40
Pattern43
Pattern8
Pattern48
Pattern49
Pattern47
Pattern41
Pattern32
Pattern27
Pattern16
Pattern4
Pattern9
Pattern12
Pattern35
Pattern34
Pattern42
Pattern45
Pattern13
Pattern46
Pattern50
Pattern30
Pattern29
Pattern24
Pattern14
Pattern5
Pattern26
Pattern3
Pattern37
Pattern39
Pattern25
Pattern38
Pattern28
Pattern17
Pattern18
Pattern22
Pattern15
Pattern21
Pattern23
Pattern20
Pattern31
Pattern36
Pattern10
Pattern33
Pattern19
Pattern44
Pattern6
Pattern1
Pattern2
cellscore
0.05
0.04
0.03
0.02
0.01
0
cell_group
Unknown
MENs
Macrophage 1
NC-Cells 1
SMC
V Endothelium
RBC
B Lymphocytes
Fibroblast 2
Fibroblast 1
T cells
NC-Cells 2
NK cells
Macrophage 2

C

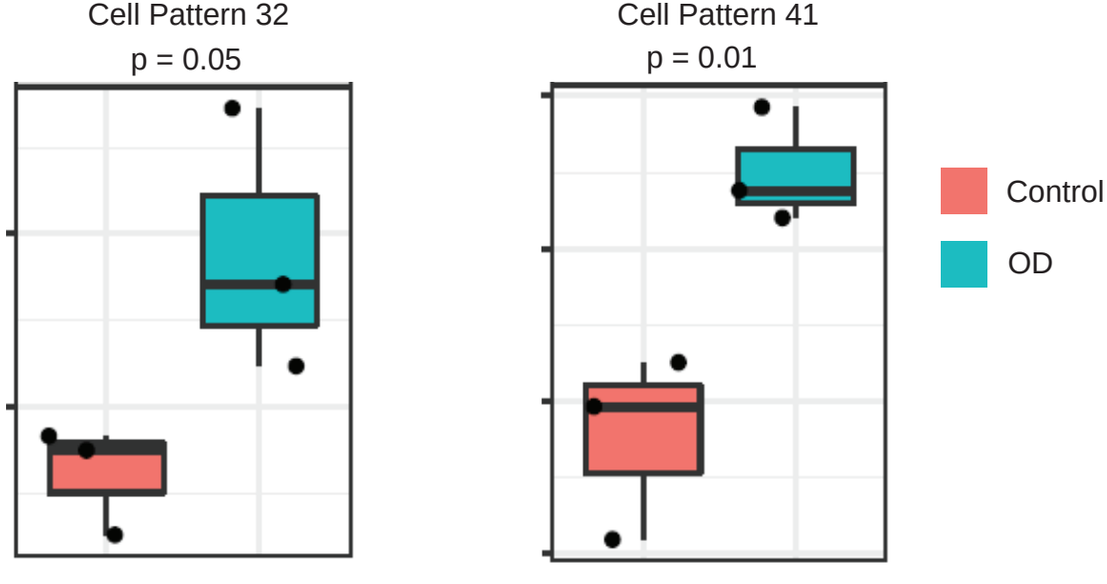
Cell Pattern 32
p = 0.05
Cell Pattern 41
p = 0.01
Control
OD